A&A 574, A102 (2015)
DOI: 10.1051/0004-6361/201423981
© ESO 2015

Astronomy & Astrophysics

Spectral classification of photometrically selected AGB candidates in NGC 6822⋆

L. F. Sibbons, S. G. Ryan, R. Napiwotzki, and G. P. Thompson

School of Physics, Astronomy and Mathematics, University of Hertfordshire, College Lane, Hatfield AL10 9AB, UK
e-mail: L.Sibbons1@herts.ac.uk

Received 11 April 2014 / Accepted 1 October 2014

ABSTRACT

Context. The ratio of C- and M-type asymptotic giant branch (AGB) stars is commonly used to estimate the metallicity of extragalactic populations. Sources in the AGB population must therefore be accurately classified as either C- or M-type. Spectroscopic data are presented for candidate C- and M-type AGB stars, previously classified using *JHK* photometry, in the Local Group dwarf galaxy NGC 6822.

Aims. This paper aims to evaluate the success of the *JHK* classification criteria used in order to determine the level of error associated with this method, and to refine the criteria for future studies. The success rate of a second independent method of source classification, the CN–TiO method, is also examined. We also review the validity of the 4 kpc radial limit imposed in our previous work.

Methods. Spectra of 323 sources, distributed across an area of 2 deg^2, were taken using the AAOmega multi-fibre spectrograph on the Anglo-Australian Telescope and have been classified using an automated classification system and spectral standards from the literature. Nearly half (135) of these sources were selected in common with a photometric catalogue that relied on the CN–TiO method.

Results. Within this sample we were able to classify 158 sources, including 82 C-type giants and one anomalous M-type giant, all members of NGC 6822, and 75 foreground K- and M-type dwarf sources. All but three of the giant sources are located within 3 kpc of the galactic centre. Using this spectroscopic sample, new *JHK* photometric criteria for the isolation and classification of C- and M-type AGB stars have been derived. The error rate in the CN–TiO method, arising from stars incorrectly classified as C-type, has been estimated to be ∼7%.

Conclusions. Based on the new *JHK* classification criteria, revised estimates of the global C/M ratio, 0.95 ± 0.04, and iron abundance, -1.38 ± 0.06 dex, are presented for NGC 6822.

Key words. techniques: photometric – techniques: spectroscopic – stars: AGB and post-AGB – stars: carbon – galaxies: dwarf – galaxies: stellar content

1. Introduction

1.1. Aims of this paper

As tracers of the old- and intermediate-age population (≳1 Gyr) and producers of dust and heavy elements including carbon, oxygen, nitrogen and s-process elements, asymptotic giant branch (AGB) stars are a crucial part of understanding the chemical evolution of a galaxy. Furthermore, AGB stars move through several evolutionary phases and make a substantial contribution to the integrated light of a galaxy (Renzini & Buzzoni 1986).

During the AGB phase, mixing mechanisms dredge up triple-α processed material from the He-burning shell. This can cause the stellar atmosphere to evolve from being oxygen-rich (C/O < 1, M-type stars) through a stage where the relative amounts of oxygen and carbon are approximately equal (C/O ∼ 1, S-type stars) to being carbon-rich (C/O > 1, C-type stars). At lower metallicities the transformation from an initially O-rich atmosphere to a C-rich one is easier, as fewer dredge-up events are required (Scalo & Miller 1981; Iben & Renzini 1983). Therefore, the number ratio of C-type to M-type stars in a population, C/M, can be used as an indirect measure of the metallicity of the local environment at the time those stars formed (Blanco et al. 1978; Cioni & Habing 2005; Sohn et al. 2006).

As AGB stars are bright in the near-infrared (NIR), where the effects of dust obscuration are greatly reduced compared to optical observations, they will become increasingly important for the study of distant galaxies with forthcoming IR-optimised telescopes, where classical optical metallicity indicators will be too faint. Asymptotic giant branch stars as a population, and the C/M ratio as a method of studying them, are important tools in advancing our understanding. In order to fully exploit the C/M ratio as a metallicity indicator, there are two issues that need to be resolved. First, a better understanding of the many evolutionary mechanisms of the AGB phase, including third dredge-up, hot bottom burning, convective overshoot, etc. and how these relate to the creation of C-type stars is required. Second, a reliable method requiring only moderate amounts of telescope time is needed for selecting C- and M-type AGB stars in distant and crowded extragalactic fields. The first of these points is being steadily advanced by observational and theoretical groups (Izzard & Poelarends 2006; Stancliffe 2010; Karakas et al. 2012; García-Hernández et al. 2013), while the second is the primary aim of this article. We aim, by improving the accuracy with which AGB stars can be selected and classified using NIR photometry, and by better quantifying the error associated with this

⋆ Tables 1, and 10–13 are available in electronic form at http://www.aanda.org

technique, to pave the way for the wider application of this method.

The Local Group irregular dwarf galaxy (dIrr) NGC 6822 is similar to the Small Magellanic Cloud. Located at a distance of ∼490 kpc ($(m - M)_0 = 23.45 \pm 0.15$ mag) from the Milky Way (MW; Mateo 1998; Lee et al. 1993), NGC 6822 is the closest undisturbed dIrr galaxy beyond the Magellanic Clouds. The galaxy appears to have experienced a relatively steady rate of star formation over the last ∼11 Gyr, although there are signs of a recent increase (Clementini et al. 2003; Komiyama et al. 2003; Gallart et al. 1996), and it has a large and well studied AGB population. NGC 6822 has been the subject of multiple studies to estimate its iron abundance (Venn et al. 2001; Tolstoy et al. 2001; Davidge 2003b; Clementini et al. 2003; Kang et al. 2006).

Sibbons et al. (2012; hereafter Paper I) estimated the global iron abundance of the AGB population of the galaxy from the calculated C/M ratio; using *JHK* photometry of a ∼3 deg^2 area centred on NGC 6822 ($\alpha(2000.0) = 19^h44^m56^s, \delta(2000.0) = -14°48'06''$). Candidate C- and M-type AGB stars were classified on the basis of their magnitudes and NIR colours to obtain the C/M ratio. However, a comparison of the classifications in Paper I with those in the work of Letarte et al. (2002), who relied on the CN–TiO method to classify sources, suggested that up to ∼20% of the C-type star population may have been misclassified as M-type stars by the derived *JHK* criteria. A review of the estimated error in source classification in Paper I and the level of misclassification in the catalogue of Letarte et al. (2002), which was previously assumed to be 100% accurate, are therefore the secondary and tertiary aims of this work. Using spectra of a sample of candidate C- and M-type AGB stars common to the catalogues of Paper I and Letarte et al. (2002), the present work is the first to use spectra to examine sources that have been classified using both *JHK* photometry and CN–TiO data, with the object of quantifying the level of error associated with each technique. We examine the levels of misclassification (a C-type star classified as an M-type for example) and also the level of foreground contamination. For each technique we also examine the impact of any classification errors on the calculated C/M ratio and the iron abundance derived from it.

The remainder of the paper is arranged as follows: first we summarise the CN–TiO method as a means of identifying C-type AGB stars. Section 2 summarises the target selection, the data and the reduction process. In Sects. 3 and 4 we analyse the data and report the results, followed by a discussion and our main conclusions in Sects. 5 and 6.

1.2. CN–TiO method

The CN–TiO method (Palmer & Wing 1982; Richer et al. 1984; Cook et al. 1986) uses two broadband filters, commonly *R* and *I* (or *V* and *I*), and two narrow-band filters, CN and TiO, to classify C- and M-type sources. The TiO and CN filters typically have a central wavelengths of ∼7750 and ∼8100 Å respectively, and widths of $\Delta\lambda$140−300 Å. Temperature information is derived from the broadband filter colours ($R - I$) while the two narrow-band filters (CN–TiO) provide low resolution spectral information. When placed on a C-type star the CN filter is on a strong band of CN and the TiO filter is on pseudo-continuum (the density of spectral features means there is no true continuum in these stars). While for an M-type star the TiO filter is on a strong band of TiO and it is the CN filter that sits on pseudo-continuum (Brewer et al. 1995, 2000; Letarte et al. 2002). This leads to a clear separation between the C- and M-type sources in ($R - I$, CN–TiO) space.

The efficiency of the CN–TiO method in selecting AGB candidates has been examined in the past by Brewer et al. (1996), who analysed spectra of C- and M-type stars in M 31 classified using the CN–TiO method and found that the spectral classifications agreed very well. However, despite its previous success, the CN–TiO method does not distinguish hotter C-type stars from the general population very well, and contamination from foreground M-type dwarfs and background galaxies can be high (Groenewegen 2006; Demers et al. 2006; Letarte et al. 2002). In addition, Brewer et al. (1995) and Groenewegen et al. (2009) have noted that as the environment around an AGB star becomes increasingly polluted by dust, the redder colours of the star mean it can go undetected at optical wavelengths. This can be a problem for C-type stars in particular, and can lead to higher levels of incompleteness and a bias towards the detection of M-type stars, affecting the C/M ratio. Furthermore, CN and TiO filters are unavailable at many observatories and as many new facilities are optimised for NIR measurements, with *JHK* as standard, it is important to clearly establish criteria for and estimates of the expected level of error when selecting C- and M-type AGB stars at these wavelengths.

2. Observations and data reduction

2.1. Target selection

Target sources have been selected from potential AGB candidates that were identified using *JHK* photometry in Paper I of this series. Our photometric data were collected using the Wide Field Camera (WFCAM) on the United Kingdom Infrared Telescope (UKIRT) and were reduced using the WFCAM pipeline at the Institute of Astronomy in Cambridge. A more detailed discussion of the observations and the reduction processes is presented in Paper I and will not be repeated here. However, we note the following: (1) the Schlegel et al. (1998) extinction maps were used to correct for foreground reddening in the direction of NGC 6822, which is estimated to be $E(B-V) = 0.26$ mag (Massey et al. 1995) (no correction was applied to account for reddening variations internal to the galaxy); and (2) although astrometric and photometric calibrations of the UKIRT data were performed using the 2MASS point source catalogue (Hodgkin et al. 2009; Irwin et al. 2004) the photometric measures were not transformed into the 2MASS system. Therefore the colours and magnitudes that are quoted here refer to the WFCAM instrumental system; should they be required Hodgkin et al. (2009) can be consulted for the relevant transformation equations.

Applying the following colour and magnitude criteria to our photometric data nearly 3800 potential C- and M-type AGB sources were identified in NGC 6822; $K_0 \leq 17.41$ mag, $(J - K)_0 \geq 0.74$ mag and $(J - H)_0 \geq 0.72$ mag. The colour boundary between the C- and M-type sources was set at $(J - K)_0 = 1.20$ mag. An examination of the stellar density profiles of the AGB and red giant branch (RGB) candidate sources led us to conclude that the strongest AGB candidates lay within 4 kpc of the galactic centre. Beyond that limit it was inferred that the density of the NGC 6822 sources had dropped to a level that made it impossible to reliably disentangle them from the remaining MW foreground contamination. Therefore the candidate AGB sources were split into two groups: (1) those within 4 kpc of the galactic centre (2368 sources); and (2) those beyond 4 kpc (1387 sources). We will discuss the sources selected for follow up spectroscopy in the context

of these two groups. As the spectral data were collected using a multi-object fibre-fed spectrograph (see Sect. 2.2), we were able to target ~400 sources.

The 2368 candidate AGB stars in the inner region were cross-matched with the catalogue of Letarte et al. (2002) who had previously classified 904 C-type AGB stars in a small field lying fully within the 4 kpc radial limit, using the CN–TiO method; 635 sources were found to be common to both catalogues. From this sample of 635 stars, 68 sources within 3 kpc (all classified as M-type in Paper I) were selected for spectroscopic follow up. A further 67 sources also within 3 kpc (46 C-type, 15 M-type and six unclassified according to Paper I) were selected from the *JHK* photometric counterparts for another 235 sources belonging to the catalogue of Letarte et al. (2002). These sources were included in our target list as although they were astrometrically matched with sources in the catalogue of Letarte et al. (2002) they were excluded from our analysis in Paper I, by the stringent quality control criterion applied, which resulted in the removal of some genuine AGB stars from the sample. The six sources that were unclassified in Paper I were without a magnitude measurement in at least one of the three photometric bands. A total of 135 sources were selected for spectroscopic follow up in the inner region, all of which had been classified as C-type stars by Letarte et al. (2002).

The majority of sources in the outer region were expected to be foreground interlopers; 188 sources, all at a radial distance of ≥5 kpc were selected. The vast majority of candidate AGB sources in the outer region were classified as M-type; this is reflected in the photometric classifications of the 188 sources targeted in this region (178 M-type and 10 C-type).

Our reasoning for only selecting target sources at ≤3 kpc or ≥5 kpc is explained below. The right ascension (RA) and declination (Dec) positions quoted for our spectroscopic targets are taken directly from the catalogues of Paper I.

2.2. AAOmega data

Observations were carried out in service mode on the nights beginning 30 and 31 August 2011 using the AAOmega multi-fibre spectrograph at the 3.9 m Anglo-Australian Telescope (AAT). AAOmega has 400 fibres, up to 392 of which can be assigned to science targets or sky at one time. Each fibre has a diameter of 2.1". This instrument was ideal for our purposes as its two degree field of view allowed us to target sources across all of NGC 6822, both inside and outside the 4 kpc radial boundary.

AAOmega is a dual-beam spectrograph, splitting the light into red and blue components. During our observations, the 5700 Å dichroic was used. In the blue arm we used the 580V grating which has a wavelength range of 3700–5800 Å and dispersion of 1.0 Å pix^{-1}. In the red arm we used the 385R grating which has a wavelength range of 5600–8800 Å and a dispersion of 1.6 Å pix^{-1}. Both configurations have a resolving power of $\lambda/\Delta\lambda \sim 1300$. The majority of useful features for the classification of C- and M-type sources (i.e. the CN and TiO absorption bands) are contained in the red spectrum. The blue arm data have been useful for the study of some of our sources (Sect. 4.1.2), but the low signal-to-noise ratio (S/N) in this part of the spectrum means that for the majority of our sources the useful wavelength range is restricted to $\lambda > 5600$ Å.

As the density of high priority sources in the inner region was very high, no sources between 3–5 kpc were selected for spectroscopic follow up to make the placement of fibres on the spectrograph easier. Of the available fibres, 30 were allocated as sky fibres, six were placed on guide stars, 37 fibres could not be placed, and the remainder were placed on targets of interest. Included in our main target list were three star clusters (C2, C3 and C4) from the work of Hwang et al. (2005), the analysis of which will be the subject of another paper. Five science frames were taken in total, two on the 30 August and three on the 31 August, each with an exposure time of 1500 s. The wavelength calibration frames were taken at the beginning of each night using a He + CuAr + FeAr + CuNe lamp. Flat fields were taken at the beginning and end of each night.

The data reduction was done using version 5 of the 2d*f*dr pipeline (Saunders et al. 2004; Smith et al. 2004) to subtract the bias, divide by the flat-field, extract the spectra and wavelength-calibrate each spectrum. Emission from the night sky was removed using a median sky spectrum created from the spectra collected by the dedicated sky-fibres, although as is common with fibre spectra the sky subtraction in the region of bright sky lines was imperfect and some erroneous or false, non-stellar features may have been left in or introduced to some spectra. This is particularly noticeable around the atmospheric [O I] 5577 and 6300 Å lines and the Na I 5890 and 5896 Å lines. No telluric correction was applied, and so the O_2 *A*- and *B*-bands (7594, 6867 Å) and the H_2O (7186, 8227 Å) features are visible in all of our spectra. The five individual spectra for each source were then combined and the red and blue parts of the spectrum were spliced together at 5700 Å. There are recurring errors in the spectra at ~4584, 4740, 4764, 4772, 4890, 4911, 4990, 5000, 5354–5376 (peak ~5370), 5390, 7630, 7649, 7658, 7684, 8009, 8020, 8030, 8040, 8060 and 8069 Å due to defective pixels in the charge couple device (CCD). The same faulty pixels do not affect every spectrum, but where spurious features are present they are marked by an X in the following figures and should be ignored.

2.3. Data quality

The region between 7530–7580 Å was assumed to be representative of the red continuum, as neither C- nor M-type stars have strong features in this region, and was used to measure the S/N for each spectrum. Owing to the short exposure time and low flux levels, a number of our spectra exhibited very low S/N (<5 per pixel) and were not considered to be of sufficient quality to use in our analysis. It was also noted that a number of sources with low S/N had negative flux values at the shortest wavelengths which we attribute to poor sky subtraction. The median S/N of our 323 spectra was ~10 per pixel, and it was decided that for the majority of our analysis we would use only those sources with $S/N \geq 10$. This reduced our usable spectroscopic sample to 162 sources: 85 sources in the inner region (≤3 kpc) and 77 sources in the outer region (≥5 kpc).

The spatial distribution of all the sources that were classified in Paper I as being AGB candidates using the *JHK* photometric classification criteria are shown in Fig. 1, with all the sources for which spectroscopic data were obtained highlighted. In Fig. 2 we show the distribution of the same sources in a colour–magnitude diagram (CMD) and a colour–colour diagram.

3. Analysis

3.1. Spectral classification

The classification of C- and M-type AGB stars is dependent on the identification of particular molecular features in the spectrum

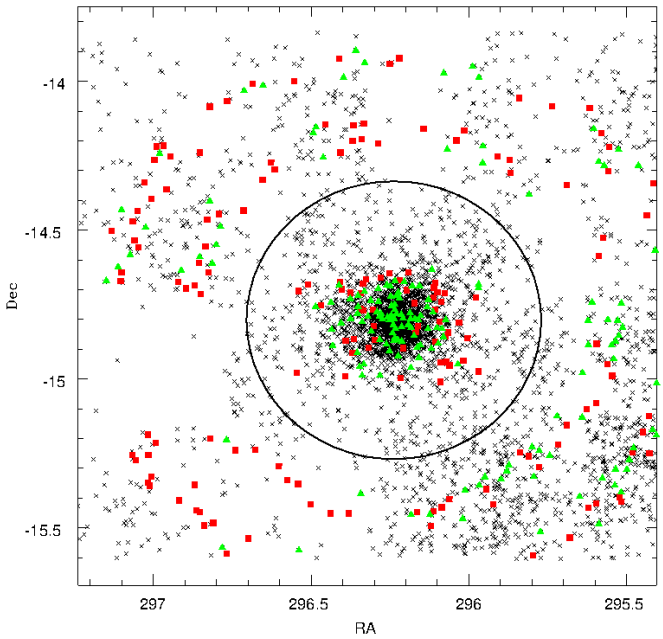

Fig. 1. Spatial distribution of all the candidate AGB sources from Paper I (black crosses). Sources for which spectroscopic data were obtained but which have $S/N < 10$ (red squares). Sources for which the spectroscopic data have $S/N \geq 10$ (green triangles). The black circle marks the position of the 4 kpc limit inferred in Paper I.

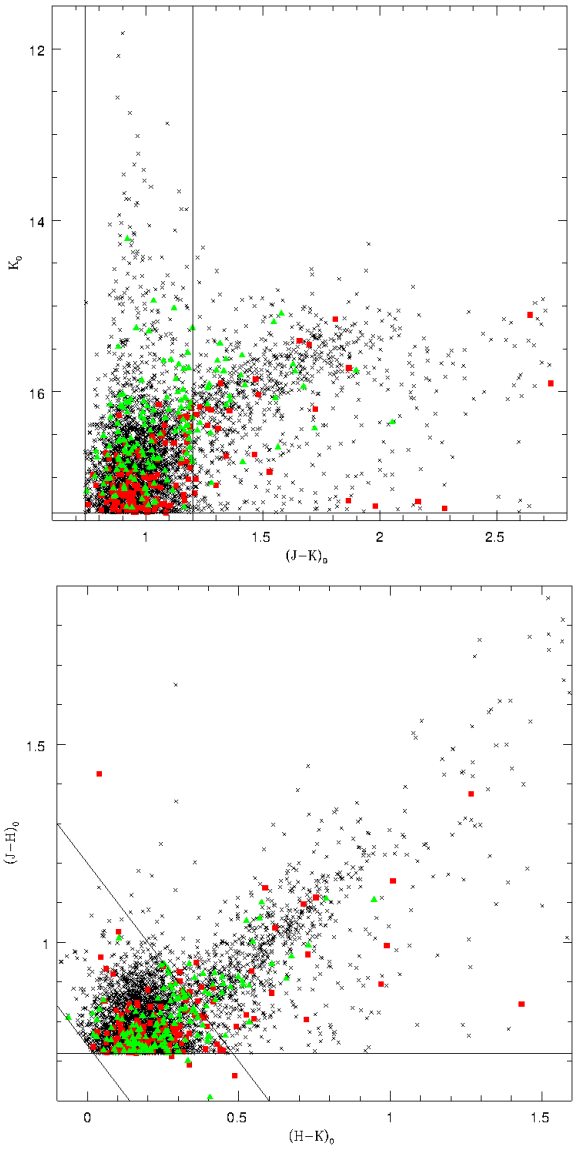

Fig. 2. *Top*: CMD of the same sources as in Fig. 1. The horizontal and vertical lines mark the position of the tip of the red giant branch and the $(J-K)_0$ colour criteria used in Paper I. *Bottom*: colour–colour diagram of the same sources. The horizontal line marks the $(J-H)_0$ colour cut used in Paper I to remove contaminating foreground sources. The diagonal lines represent the $(J-K)_0$ colour boundaries used to select C- and the M-type sources.

of the star. The spectra of M-type stars contain O-rich molecular species like titanium oxide (TiO) and vanadium oxide (VO), while C-type spectra contain carbonaceous molecules like C_2 and cyanide (CN). The bandheads of the main molecular features and other lines used for the classification of our spectra are listed in Table 1. We also include in Table 1 some of the features used to classify S-type stars – mainly zirconium oxide (ZrO) and VO – although none were detected in our sample.

The spectra presented here have been classified in two ways. First, each was classified using our spectral matching program (Sect. 3.1.1). Second, each spectrum was classified by eye.

3.1.1. Automated spectral classification

To ensure that our spectra were classified in a consistent and objective fashion, it was decided to attempt to automate the classification process. This was done by comparing 2–3 regions in each of our spectra with the same regions in spectra of known type taken from standard libraries in the literature. The goodness of the match between the two spectra was assessed using a χ^2 test.

The regions selected for comparison were 1) 5820–6750 Å; 2) 6900–7500 Å; and 3) 8170–8210 Å (Fig. 3). The wavelength ranges of regions 1 and 2 were chosen to include the strong molecular features of TiO and CN, and to exclude the atmospheric O_2 bands. Certain luminosity indicating features are also present in regions 1 and 2, but region 3 was chosen specifically for this purpose and includes the Na I (8183, 8195 Å) doublet. All three regions were compared with the chosen library spectra where possible. The standard spectra used for comparison were selected from the libraries of Danks & Dennefeld (1994) and Kacharov et al. (2012), both of which can be obtained through the VizieR database.

The spectral library of Kacharov et al. (2012), which contains spectra of 546 sources at a resolution of 12–13 Å in the wavelength range of 5000–10 000 Å was particularly useful, as it is the largest spectral library of AGB sources in NGC 6822. It includes M-type giants of subclass M, M0, M0.5, M1, M2, M3, M4, M5, M6 and M6.5, S-type giants of subclass S0 and S4, and C-type giants of subclass C, C3.2, C5.5, C6.5 and C8.2; as well as foreground K-type (dK, dK7) and M-type (dM, dM0, dM1, dM1.5, dM2, dM3, dM3.5, dM4, dM4.5, dM5, dM6) dwarf stars in the direction of NGC 6822. Unfortunately, owing to the effects of severe fringing at redder wavelengths, Kacharov et al. (2012) suggest that the useful wavelength range of their spectra is limited to 5000–7800 Å. We did not rely on their data beyond ~7500 Å. This meant that we were only able to compare features in regions 1 and 2 when matching our spectra to those of Kacharov et al. (2012).

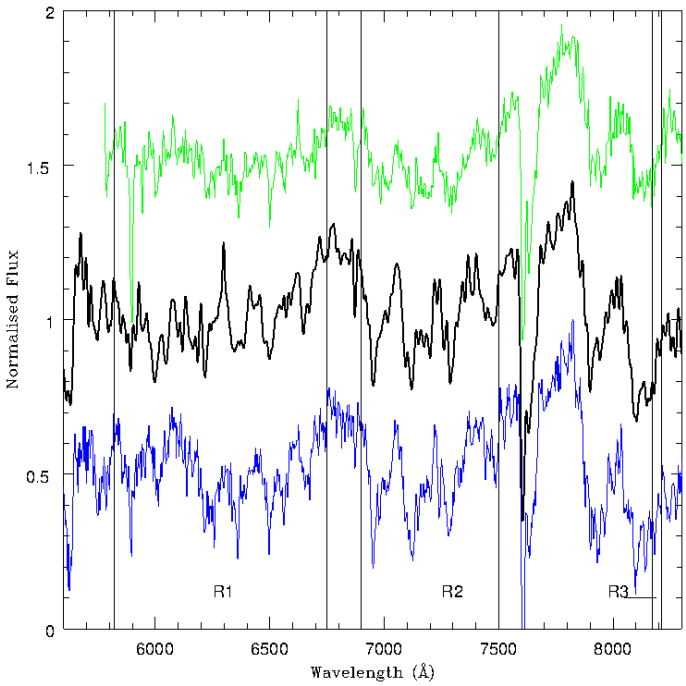

Fig. 3. Three spectra that have been normalised and had their slopes realigned for comparison. In the middle is the spectrum for one of our sources, ID: 211898 (black line). Top is the spectrum from Danks & Dennefeld (1994) (green line) and bottom is the spectrum from Kacharov et al. (2012) (blue line) that were selected as being the best match for our spectrum by the χ^2 matching program – both are C-type stars. The vertical lines mark the boundaries of regions 1, 2 and 3 as discussed in the text (Sect. 3.1.1).

The assessment of features in region 3 of our spectra relies on comparisons with the spectral standards of Danks & Dennefeld (1994). Danks & Dennefeld presented a catalogue of spectra for 126 sources, but only included one S-type star and two C-type stars, with no subclass given. The Danks & Dennefeld (1994) spectra cover the wavelength range 5800–10 200 Å with a dispersion of 4.3 Å pix^{-1} from which we assumed a resolution of ~9 Å.

In order to compare our spectra with those in the spectral libraries, each of our spectra was first normalised to the median flux value between 7530–7578 Å and then smoothed to the same resolution and interpolated on to the same wavelength scale as the comparison spectrum. The spectrum being used for comparison was also normalised, and both spectra were then truncated to the wavelength range 5800–8250 Å. The upper wavelength limit was reduced when the comparison spectrum did not extend far enough into the red.

To ensure that only the molecular or line features, and not the slope (which may be affected by the metallicity of the star, reddening variations in the foreground, different instrumentation and the data reduction processes used) would be used to determine how well the two spectra matched, the slope in the continuum level of our spectrum was realigned to match that of the comparison spectrum. This was done by dividing the unclassified spectrum by the standard, and then making a linear fit through regions 1, 2 and 3. Then by dividing our spectrum by the fit we were able to realign it with the standard. This was important, as the slope of stars of the same spectral classification in the libraries of Danks & Dennefeld (1994) and Kacharov et al. (2012) were sometimes very different.

Regions 1, 2 and 3 (where possible) in the unclassified spectrum were then individually compared to the same regions in the standard spectrum using a χ^2 test. The flux error values obtained during the reduction process, were used in the calculation of χ^2 for each region. The χ^2 value for each region was then summed to provide a total χ^2 value which was used to assess the goodness of the match between the unclassified and the standard spectra. This process was repeated so that each of our spectra were compared with every spectrum in the libraries of Danks & Dennefeld (1994) and Kacharov et al. (2012). Once every potential match to the unclassified spectra had been assessed, the *best* match (i.e. the match with the lowest χ^2), from each library of standards was identified. Figure 3 shows one of our spectra (ID: 211898) and the spectra from the spectral libraries of Kacharov et al. (2012) and Danks & Dennefeld (1994) that were assigned as being the best match. We have not attempted to attach significance levels to our derived χ^2 values, as because of the multiple manipulations of our spectra, the errors associated with each point are no longer independent and the distribution is unlikely to be Gaussian.

Although the χ^2 test may present us with the best match for our spectrum from the list of spectral standards provided, we are aware this may not necessarily be the *right* classification. Therefore, each classification was checked by eye against the suggested best matches, Fig. 3, and also against the spectral standards given in the "Atlas of digital spectra of cool stars" by Turnshek et al. (1985). The visual inspection also allowed us to identify any noteworthy features present in the spectrum, such as emission lines which are present in about a quarter of our spectra (see Sects. 4.1.2 and 4.2.2).

The spectral classifications assigned by the matching program were confirmed by eye in the majority of cases. In the outer region the automated classification was confirmed in 81% of cases when using the spectral library of Danks & Dennefeld (1994) and in 95% of cases when using the spectral standards of Kacharov et al. (2012). In the inner region, the situation was more complex: overall when using the library of Danks & Dennefeld (1994) our visual inspection agreed with that of the matching program for 49% of the spectra and for the Kacharov et al. (2012) library the agreement level was 65%. The lower success rate of the matching program in the inner region was traced back to a subset of the stars that were classified as K-type dwarf stars when using the Kacharov et al. (2012) library and primarily as K-type giants when using the Danks & Dennefeld (1994) library. Upon visual inspection of these sources, weak CN features were detected and 26 sources were reclassified as C-type giants. The consistency with which these sources were classified as K-type stars in comparison to the successful classification of several more C-type sources suggests that these sources do form a distinct group, as we discuss in Sect. 3.1.4. If these sources are excluded when comparing the automated and by eye classifications of sources in the inner region, the agreement increases to 72% when using the Danks & Dennefeld (1994) and 93% when using the Kacharov et al. (2012) library.

3.1.2. Luminosity classification

While the molecular bands of CN and TiO provide robust criteria for the classification of a source as either a C- or M-type, the distinction between luminosity types is more difficult. In other studies, the radial velocities or proper motions of individual stars have been used to differentiate between extragalactic giants and foreground dwarfs. However, the relatively low resolution of our spectra and the small difference between the radial velocities

of NGC 6822 and the MW (~44 km s^{-1}; Battinelli et al. 2006) meant we could not use radial velocity to distinguish between foreground (MW) dwarfs and distant (NGC 6822) giants at a star by star level. The situation for proper motion is the same, where PPMXL (Roeser et al. 2010) has insufficient accuracy to distinguish between Galactic and extragalactic stars in this direction. However, because of the large number of stars in our spectral sample it has been possible to determine the mean radial velocities of those stars in the inner (i.e. less than 3 kpc from the galactic centre) and the outer (i.e. more than 5 kpc from the galactic centre) regions quite well. Radial velocities were determined separately for each night for stars with $S/N \geq 10$, using IRAFs fxcor cross-correlation technique using two templates: a C-like star and an M-like star with higher than average counts. As the spectrograph had been configured primarily for deriving spectral types from broad molecular bands over a wide wavelength range, the spectra were not optimised for accurate radial velocity measurements, but nevertheless the narrower, Ca I infrared triplet lines were found to give a tolerable cross-correlation signal. The stars in the inner region were found to have a mean heliocentric radial velocity of -40.4 ± 4.2 km s^{-1}; the uncertainty quoted is the standard error in the mean. The stars in the outer region, which we expect to be predominantly MW foreground stars, were found to have a mean heliocentric radial velocity of -1.1 ± 8.8 km s^{-1}. The difference between the two subsamples is therefore -39.3 ± 9.8 km s^{-1}, i.e. significant at the 4.0σ level.

This result may be subject to some revision in follow up work which is currently in progress and will be presented in a subsequent paper. However, it still provides kinematic evidence in support of the findings we presented in Paper I, that the stars more than 4 kpc from the centre of NGC 6822 mostly belong to the foreground. Although, it cannot be used to identify individual foreground stars in our sample. For that purpose we have relied on the presence of spectral features and comparison with spectral standards to confirm the luminosity class assigned to our spectral sources by the automated matching program. For example, in M-type stars the presence and strength of some spectral features can be used to discriminate between dwarf and giant stars, like the Na D lines which are greatly enhanced in M-type dwarf stars in comparison to M-type giants. Hydride features (e.g. CaH, MgH) are also stronger in dwarf stars due to their higher surface gravity. The wavelength range of region 3 was chosen specifically to target the Na I doublet at 8183 and 8195 Å. However, we have also relied on the presence and strength of the following features; the Ca I line at 6162 Å, the Na I doublet blend at 5890 and 5896 Å and the MgH bandhead at 5211 Å during our automated and by eye classifications. These identifiers were selected as the MgH bandhead is a strong feature in the spectra of late K- and M-type dwarf stars, and while both the Na I doublets are seen in the spectra of giant stars they are stronger in dwarf sources. However, as the Na I D-line is also seen in the spectrum of the night sky it must be treated with caution. The Ca I line is also enhanced in dwarf stars in comparison to giants. All four features are present and marked on the average dM0 spectrum (see Sect. 3.1.4) presented in Fig. 4.

Although the increasing levels of noise at bluer wavelengths and poor sky subtraction in our spectra mean that it has not always been possible to identify all of these features in every spectrum, the presence of at least 2–3 has provided the basis for the classification of dwarf stars in our spectroscopic sample. While the classification of some of the sources as dwarf stars is not as robust as we would wish, we are confident, based on our automated and by eye classifications, that our classifications are correct.

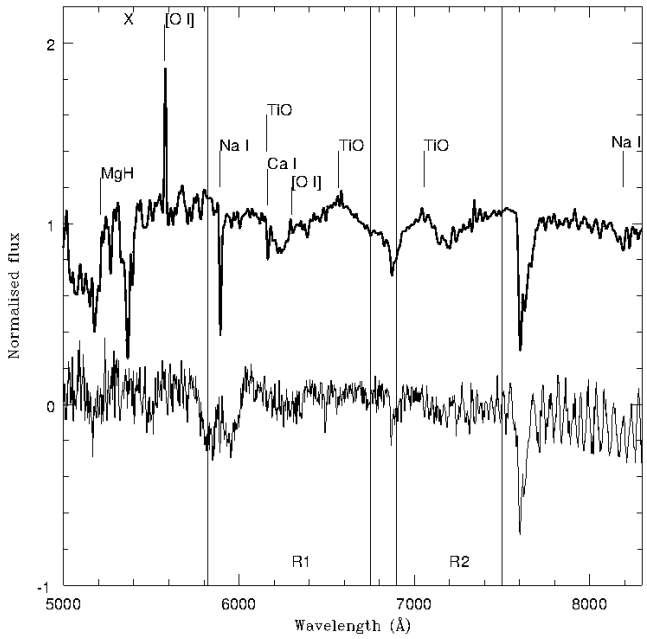

Fig. 4. Average spectrum (see Sect. 3.1.4) for the sources classified as dM0 is shown (top). The molecular bandheads and line features used to identify the dwarf sources in our spectroscopic sample are marked. For comparison we show (bottom) the spectrum of a M0 III star from Kacharov et al. (2012). R1 and R2 refer to classification regions 1 and 2.

3.1.3. Colour ratios

As an independent check on the luminosity classification of our sources, we applied the colour ratios of Kirkpatrick et al. (1991). Kirkpatrick et al. presented spectra of 77 dwarf stars (K5–M9) and 14 giant and super-giant sources (K5–M5) at a resolution of 18 Å in the wavelength range 6900–9000 Å. As part of their analysis they used colour ratios to distinguish between luminosity classes. Colour ratios are calculated using the ratio of the summed flux in two regions of the spectrum, one containing a feature of interest that can be used as a luminosity indicator and a second relatively featureless region that is used as proxy for the continuum. Kirkpatrick et al. (1991) defined four such ratios, *A* to *D*, which we list in Table 2.

When applying these ratios to our own data ratio *C* and two ratios of ratios, *B*/*C* and *D*/*C*, showed a distinct separation between those sources we classified as giants and those we classified as dwarf stars. The calculated ratios for each source are plotted against its $(J-K)_0$ colour, which we have used as representative of spectral subclass of the two luminosity types, in the three panels of Fig. 5. In each plot we have also shown the line which we have judged, by eye, best separates the dwarf and giant sources with the minimum of cross contamination.

Ratio *C*, shown in the top panel, shows the cleanest separation between the two luminosity types. The position of the one potential M-type giant in our sample has been marked on the plots shown in Fig. 5. However, as this is the only such source in our sample and because of anomalies in its spectrum (see Sect. 4.1.4), we cannot draw any conclusions about the ratio *C* distribution of M-type giants; although we speculate that apart from bluer $(J-K)_0$ colours the ratio *C* distribution of the M-type giant population would not be too dissimilar from that of

Table 2. Summary of the four colour ratios defined by Kirkpatrick et al. (1991).

Ratio	Feature measured	Numerator	Denominator
A	CaH (6975 Å)	7020–7050 Å	6960–6990 Å
B	Ti (7358 Å)	7375–7385 Å	7353–7363 Å
C	Na I (8183, 8195 Å)	8100–8300 Å	8174–8204 Å
D	Ca II (8542 Å)	8567–8577 Å	8537–8547 Å

the C-type stars which have values between 0.70 and 1.01. The K- and M-type dwarf sources in our spectral sample show a narrower distribution than the giants, between 0.98−1.20 (the majority of which have ratio $C > 1.06$). The distribution of ratio *C* values for the two types of dwarf are very similar.

Kirkpatrick et al. (1991) noted that for the individual ratios *A* and *C*, both of which rely on features which are stronger in dwarf stars than in giants, that the giant sources lay below the dwarf sources when the ratio was plotted against spectral type. For ratios *B* and *D*, which rely on features which are stronger in giant stars, the situation was reversed. They therefore sought to enhance the separation between the two luminosity types by using ratios of the individual colour ratios. We have applied these ratios of ratios and found them useful, but note that they work less well for early type spectral sources as the individual ratio values for the different luminosity types are quite similar – especially for ratio *A*. We present the two ratios of ratios that we found best separated the giant and dwarf sources in our sample, *B*/*C* and *D*/*C*, in the middle and bottom panels of Fig. 5.

The colour ratio's of Kirkpatrick et al. provide a useful confirmation of the luminosity classifications we assign to our spectral sample. More generally however, the use of these ratios as a tool to discriminate between different sources types in large photometric surveys is limited by the availability of the required narrow band filters and the throughput of those filters.

3.1.4. Average spectra

Once the automated classifications were checked by eye, sources which had been assigned to the same spectral subclass when using the library of Kacharov et al. (2012) were compared to ensure they were consistent. The top panel of Fig. 6 shows an example of this for sources classified as dM3.5; each spectrum has been normalised and then plotted with a slight offset, in order to compare all of the dM3.5 spectra with each other and with a dM3.5 spectrum from Kacharov et al. (2012). Once satisfied that all the sources classified as a particular spectral type were consistent with one another, an average spectrum was created for each type in order to reduce the random noise in the spectrum. For those sources classified as dM3.5, the average and a standard spectra can be seen in the bottom panel of Fig. 6. For the purposes of comparison, the average spectrum has been smoothed to the same resolution as the standard spectrum; this has the additional benefit of increasing the S/N per resolution element. However, the average dM3.5 spectrum, and other average spectra presented are still affected by dead pixels on the CCD and poor sky subtraction around some telluric emission lines. As can be seen in Fig. 6, the agreement between the average spectrum for the sources classified as dM3.5 and the dM3.5 standard spectrum is good. The presence of key molecular TiO bandheads (~6159, 6569, 7054 Å) can be clearly seen in the average spectrum, as can the CaH band (6386 Å). Also seen in the average spectrum, though less obvious in the standard

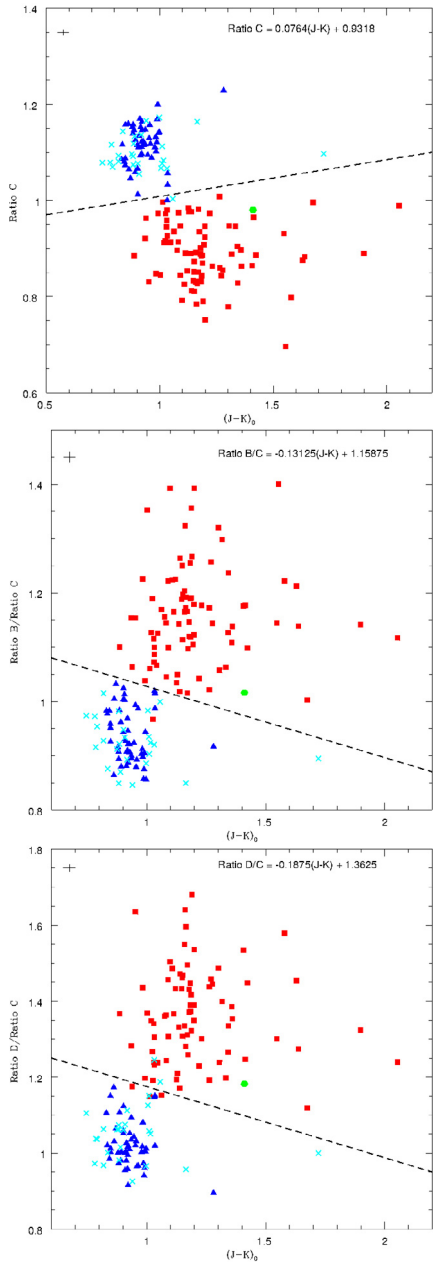

Fig. 5. *Top*: ratio C vs. $(J-K)_0$ for our spectroscopically classified sample. Symbols are as follows: red squares – C-type giants, blue triangles – M-type dwarfs, cyan crosses – K-type dwarfs and green hexagon – M-type giant (see Sect. 4.1). *Middle*: ratio B/ratio C vs. $(J-K)_0$. *Bottom*: ratio D/ratio C vs. $(J-K)_0$. In the top left corner of each plot we show the typical error bars associated with the $(J-K)_0$ colour and measured ratio of each point. In each panel the diagonal dashed line marks the estimated separation between the two luminosity types.

spectrum due to fringing, is the widening and deepening redward of the O_2 A-band due to strengthening TiO bands in that region.

The same procedure was repeated for all of our spectra. In Fig. 7 we present the average spectrum for each of the different spectral subclasses found in our sample for the C-type giants and the M- and K-type dwarfs. Identifying spectral features have been marked in each panel. However, we note that the spectral subclasses assigned to the spectra in our sample by the matching program should be treated with caution for two reasons; first as the spectra in the library of Kacharov et al. (2012) were classified

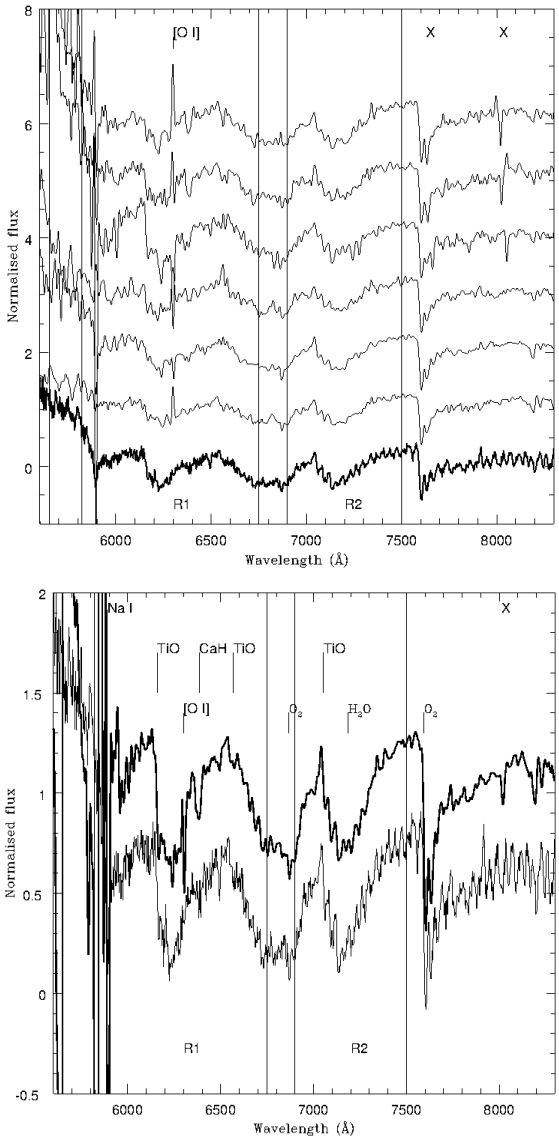

Fig. 6. *Top*: six of the seven spectra classified as dM3.5 by the automated matching program are presented with a dM3.5 standard spectrum from Kacharov et al. (2012) (thick black line). The seventh source (ID: 128222) classified as dM3.5 was excluded because of excessive noise in the blue which obscured the plot. *Bottom*: the average (thick solid line) of all seven spectra classified as dM3.5 including source ID:128222, and the same dM3.5 spectrum from Kacharov et al. (2012) (thin solid line). Our spectra have been smoothed to the same resolution as the Kacharov et al. (2012) data (in both panels) for comparison purposes.

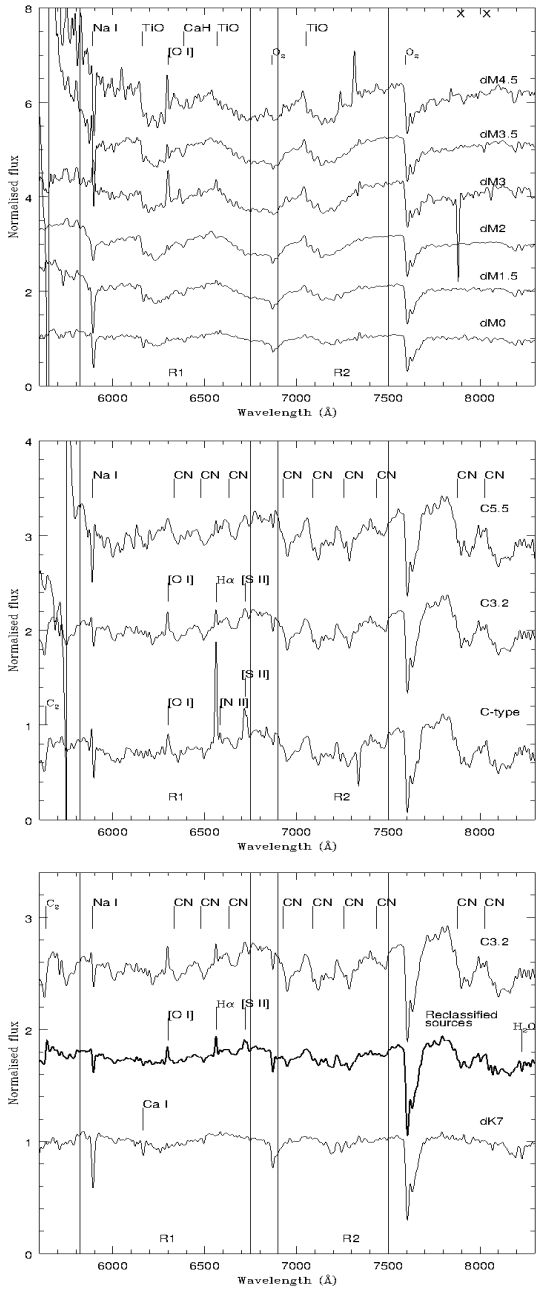

Fig. 7. *Top*: average spectra of the different subclasses of M-type dwarf identified in our spectral sample. *Middle*: average spectra of the most common types of C-type giants identified in our sample. *Bottom*: average spectrum of the genuine dK7 sources in our sample and the average spectrum of those sources classified as K-type dwarf stars by the matching program but which were reclassified as early C-type stars (bold line) following a visual inspection. The C3.2 average spectrum is plotted again for comparison.

based on comparisons with MW sources (Jacoby et al. 1984; Turnshek et al. 1985), which have a higher average metallicity than those in NGC 6822, it may have resulted in too late a subclass being assigned to some of their spectra, a concern which they note themselves. If this is the case this error would propagate to our own classifications. Second, the matching of one of our spectra to one in the library of Kacharov et al. (2012) (or Danks & Dennefeld 1994), is dependent on the types of spectra present in that library. As the Kacharov et al. (2012) library does not contain a full set of M- and K-dwarfs or C-type stars of every subclass and luminosity class, we cannot assume that a source classified as C3.2 truly belongs to that subclass but rather that the spectrum of that source is more similar to that of a C3.2 star than a C5.5 star. For these reasons although the initial classification of our spectra by our matching program has been very successful, we do not necessarily assume that the subclass is correct. However, these subclasses are probably indicative of the differing spectral subclasses of these sources.

In the top panel of Fig. 7 the average spectrum for the different subclasses of M-type dwarf in our spectral sample are shown. The increasing strength of the TiO bands between dM0 and dM4.5 suggests that the division of the sources used to build the average spectra was accurate. The middle panel shows the average spectrum for each of the most common types of

C-type star detected in our sample, C3.2, C5.5 and the more general C-type. The average spectrum labelled as C-type has been created using sources that were matched with the C spectrum in the library Kacharov et al. (2012). Although Kacharov et al. (2012) gives no information about the subclass of this spectrum, from the strength of the CN features we suggest that this spectrum is consistent with an early to mid C-type star, similar to a C3.2. Interestingly all of these sources classified as simply C-type show emission lines; these lines are enhanced in the average spectrum where we identify Hα and the [S II] doublet (see Sects. 4.1.2 and 4.2.2 for further details). The [O I] (6300 Å) line is also visible but this is probably the result of poor sky subtraction rather than a real feature. Comparing the average spectra for the C3.2 and C5.5 sources, we again see the strengthening of distinguishing molecular features, in this case the CN bands. An average spectrum for those sources classified as C8.2e is not shown here as there are only two such sources in our sample, an insufficient number to build up a useful average spectrum.

In the bottom panel of Fig. 7 we present an average spectrum for those sources classified as dK7 by the matching program and that were confirmed to be K-type dwarf stars following our visual inspection. While we cannot compare the dK7 average spectrum to other dwarf K-type spectra of a different subclass, the average is consistent with the spectra of K-type dwarfs in the spectral catalogues mentioned above. We do not show an average spectrum for those sources classified as dK, as their number was insufficient to create a useful average spectrum. In the same panel we also show the average spectrum for those sources which were initially classified as dK7 or dK by the matching program but which we later reclassified as C-type stars (26 sources, all located in the inner region). The average spectrum for these sources shows, like the individual spectra, that while the CN bandheads at 7876 and 8026 Å are present, and those at 6925, 7088, 7259 Å and possibly 7437 Å are emerging, they are weak compared to those in the C3.2 average spectrum. This may be because these stars are of an earlier subclass. We note that the average dK7 spectrum can be distinguished by the presence of a distinct Ca I (6162 Å) absorption line which is not seen in the average spectrum of those stars which were reclassified. The average spectrum of the reclassified C-type giant stars on the other hand shows the C_2 (5636 Å) bandhead, which is seen in the C3.2 average but not in the dK7 average.

As to why these sources were classified as dK or dK7 by the matching program, we suggest that their weak CN features may have resulted in poor χ^2 values being derived when comparing them with the C-type spectra in the library of Kacharov et al. (2012), the earliest of which is C3.2. An attempted match with the M-type spectral standards in that library would also have resulted in poor χ^2 values. As a result it is possible that the relatively featureless spectra of the dK and dK7 standards provided the best χ^2 value with the result that these early C-type sources were misclassified as late K-type stars.

In Table 10 we present the final spectral and luminosity classification for all the sources in the inner region, along with some photometric data. The data are presented as follows, in Col. 1 the unique ID number of the source is given, Cols. 2 and 3 list the RA and Dec (J2000), Cols. 4–6 list the reddening corrected magnitude of the source in J, H and K magnitude, Cols. 7 and 8 list the photometric classification of the source and its distance from the galactic centre (according to Paper I). Columns 9–11 list the source's final spectral classification and the spectral classifications (including subclass) assigned by the matching program when using the spectral libraries of Kacharov et al. (2012) and Danks & Dennefeld (1994) respectively. In Cols. 12–14 we list the ID number for the source in the catalogue of Letarte et al. (2002) and the values they give for $(R-I)$ and (CN–TiO). Lastly in Col. 15 we list the S/N for each spectrum. With the exception of the data from Letarte et al. (2002) the same information is listed in Table 11 for the outer region sources.

3.2. Poor quality data

As stated in Sect. 2.3, we retained for analysis only those spectra with $S/N \geq 10$. However, of the 161 spectra collected with S/N below this threshold, a small number displayed features that were sufficiently strong at wavelengths $\lambda > 6000$ Å that we were able to make a tentative classification. Using the techniques discussed above we have classified a further 43 sources (32 in the inner region and 11 in the outer region) with $S/N \sim 7$–10. Data for these sources are presented in Table 12 in the same format as in Table 10. The remaining 118 sources in our original spectroscopic sample were too noisy and the important spectral features could not be distinguished, as a result these sources could not be classified.

4. Results

We now assess the success with the which the colour and magnitude criteria determined in Paper I (Sect. 2.1) correctly categorised the sources in our spectroscopic sample. By reviewing the colour and magnitude distributions of sources with confirmed spectral type, we can improve the criteria for the selection of C- and M-type AGB stars when using NIR photometry, and provide an estimate of the error associated with this method and our original criteria. As many of our targets were selected in common with the catalogue of Letarte et al. (2002) we are also in a position to assess the success of the CN–TiO method and make the first estimate of the associated error.

4.1. Inner region sources

For the 85 sources in the inner region for which we collected sufficiently high quality data, we have been able to classify 83 of the spectra. We identified 79 C-type giants, one potential M-type giant, one M-type dwarf and two K-type dwarf stars; we were unable to classify two sources. A summary of these spectral classifications compared to the photometric classifications assigned to these sources in Paper I is shown in Table 3.

The only oxygen-rich giant source in our spectroscopic sample is described as a potential M-type giant due to anomalies in its spectrum (Fig. 8). The spectral regions labelled R1 and R2 contain strong absorption bands resembling the TiO 6159 and 7054 Å bandheads, seen in the M-type stars. However, the TiO 6569 Å bandhead is unclear or absent. More unusually, at $\lambda > 7500$ Å where the CN and TiO filters discriminate, the spectrum appears to show the CN 7876 Å and 8026 Å bands. Furthermore, the telluric O_2 A-band shows little sign of the red extension associated with TiO 7628 Å. Because of the unusual nature of this spectrum and the crowding issues near the centre of the galaxy we considered the possibility that light from a source other than the intended target had been captured in this spectrum. Within our own catalogues the closest neighbouring source was ~2″ away. As this is nearly double the radius of the instrument fibres we concluded that even the closest of the neighbouring sources was unlikely to have contaminated the spectrum of our apparent M-type giant. However, there may be one or more

Table 3. Summary of the classifications assigned in this work, and in Paper I, to the 85 ($S/N \geq 10$) sources in our spectral sample for the inner region.

Spec. type	Phot. type (Paper I)				
	M-type giant	C-type giant	RGB	Foreground	Excluded
M-type giant	0	1	0	0	0
C-type giant	54	24	0	0	1
M-type dwarf	1	0	0	0	0
K-type dwarf	2	0	0	0	0
Unclassified	1	0	0	0	1

Notes. The column headed as excluded refers to those sources that were excluded in Paper I due to the quality flag criterion used.

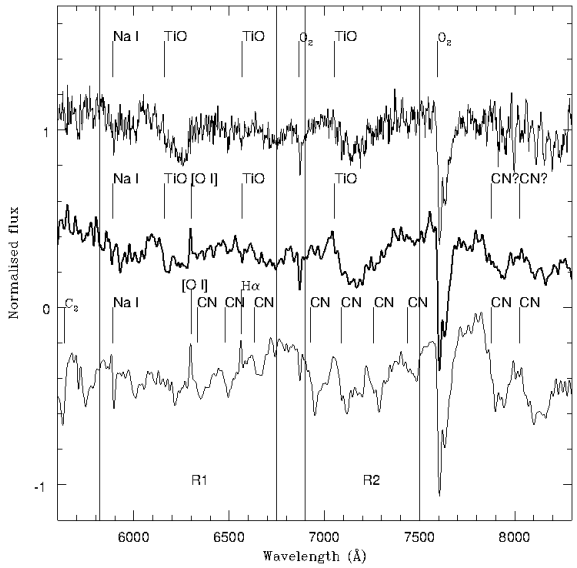

Fig. 8. Spectrum of source ID: 197590 (bold line), ID: 788 in the catalogue of Letarte et al. (2002). This star has been spectroscopically classified as an M-type giant, but also shows CN features. Above is plotted the spectrum of an M1 III star, from the catalogue of Kacharov et al. (2012) for comparison. Below is plotted the average C3.2 spectrum. The TiO and CN bandheads, and other molecular and atomic features, have been marked.

other sources, of which we are unaware, either in NGC 6822 or along the line of sight, that may have contaminated the spectrum. On the other hand, if this unusual spectrum does originate from a single source, the anomalous features we observe indicate why Letarte et al. classified the source as a C-type star and why we hesitate to classify it as an M-type giant. The true nature of this star remains a mystery, but for the remainder of this work we shall regard it as an M-type giant (the only one in our sample), however it is clearly not representative of that population.

4.1.1. *JHK* photometric colours

In the left hand panels of Fig. 9 we present a CMD and a colour–colour diagram of all the spectroscopically confirmed sources in the inner region. In the CMD we can see that the C-type giant population extends significantly blueward of the $(J-K)_0 = 1.20$ mag colour boundary imposed in Paper I. On the other hand the one potential M-type giant we have identified sits redward of the $(J-K)_0$ colour separation with a colour of $(J-K)_0 = 1.41$ mag. This confirms that there is a significant overlap between the $(J-K)_0$ colours of C- and the M-type AGB sources in NGC 6822. The C-type population covers a colour range of $0.89 < (J-K)_0 < 2.05$ mag with the peak of the colour distribution falling between 1.10–1.20 mag. Approximately 70% of the 79 spectroscopically confirmed C-type stars have $(J-K)_0$ colours bluer than 1.20 mag, although only 9% of sources have $(J-K)_0$ colours of less than 1.0 mag (we note that we preferentially targeted stars having $(J-K)_0 < 1.20$ mag but that were classified by Letarte et al. as C-type stars, so this colour distribution is not unbiased). It can be clearly seen in Fig. 9 that the C-type giant sources form a diagonal branch toward redder colours from around $(J-K)_0 \sim 1.0$ mag, with a general trend toward brighter magnitudes at redder colours.

The bottom left hand panel of Fig. 9 shows a $(H-K, J-H)_0$ colour–colour diagram of the spectroscopic sample in the inner region. With two exceptions, all of the C-type sources in the spectroscopic sample have $(J-H)_0$ colours redder than 0.72 mag. This is a reflection of the colour criterion applied to the photometric sample from which our spectroscopic targets were selected; however we do note that ~70% of the C-type sources have $(J-H)_0 \geq 0.8$ mag. The first of the exceptions (ID: 216688) was astrometrically matched with a source in the catalogue of Letarte et al. (2002) and so was included in our spectroscopic sample although it was originally rejected from the photometric catalogues of Paper I due to its quality flag classifications. The second exception (ID: 204144) was also rejected in Paper I due to the quality of its photometry and as no J-band magnitude has been recorded for this source we cannot derive a value of $(J-H)_0$.

The three spectrally confirmed dwarf sources detected within the inner region display a much narrower range of *JHK* colours and magnitudes. Collectively the M- and K-type dwarf stars have a $(J-K)_0$ colour range of 1.01−1.13 mag and a $(J-H)_0$ colour range of 0.70–0.78 mag. The number of dwarf sources in the inner region is too small to place any strong constraints on the colours of the foreground population but it will make an interesting comparison with the colours of the larger dwarf population in the outer region (Sect. 4.2.1).

4.1.2. Emission line stars

During our visual inspection of the spectra it was noted that about a quarter of our main sample of 162 sources showed Hα in emission. In addition to Hα, 25 stars (20 in the inner region and 5 in the outer region) showed forbidden emission lines (e.g. [S II],[N II]) in their spectra. These sources are denoted by an e in their classification in Tables 10 and 11. A further 15 sources (11 in the inner region and 4 in the outer region, see Table 4) also showed [O III] and Hβ in the bluer part of the spectrum between 4800–5050 Å. The presence of forbidden lines was unexpected as they suggest low density, high energy environments around these stars which are not consistent with those expected around

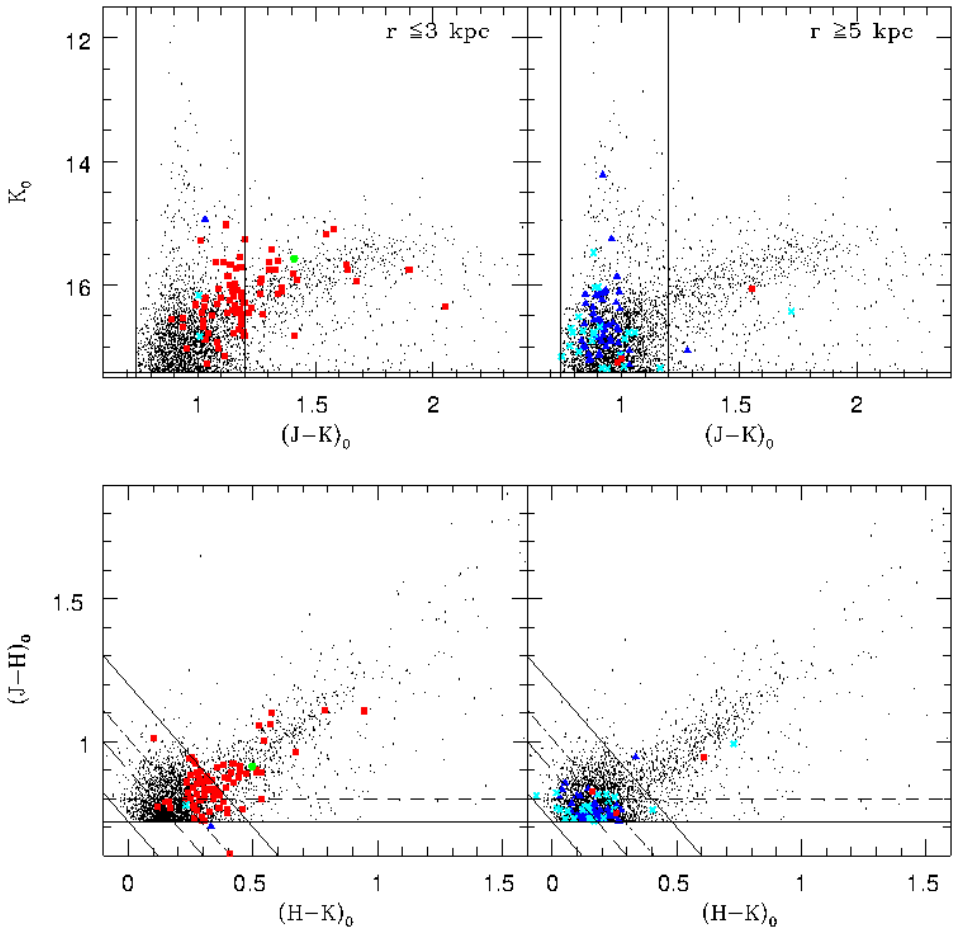

Fig. 9. *Top*: CMDs of all the spectroscopically identified sources ($S/N \geq 10$) overlayed on the AGB candidate sources classified in Paper I. *On the left* are sources from the inner region (≤3 kpc) and *on the right* are sources from the outer region (≥5 kpc). The symbols used are the same as in Fig. 5. The solid horizontal and vertical lines mark the selection criteria used in Paper I. *Bottom*: colour–colour diagrams of the same sources. The solid diagonal and horizontal lines mark the selection criteria used in Paper I. The dashed horizontal line marks an alternate colour criterion at $(J-H)_0 = 0.80$ mag discussed in the text. The long dash diagonal line and the dash-dot diagonal line represent the blue limits used by Kacharov et al. (2012) and Bessell & Brett (1988) respectively to try to eliminate foreground sources.

AGB or late dwarf stars. We have been unable to categorically classify these emission line sources, but we outline our thoughts here, beginning with those sources in the inner region.

Low ionisation sources

All but one (ID: 206129) of the emission line sources in the inner region were classified as C-type, meaning that they clearly showed the molecular features of CN and C_2 as well as emission lines. Source ID: 206129 was classified as a K-type dwarf star and hence a foreground contaminant in our sample, therefore we will not consider it further in this section but will discuss it with the other dwarf emission line sources in Sect. 4.2.2. We considered two possible explanations for the C-type sources which show Hα and the low ionisation lines[1] of [S II] and sometimes [N II]: first that the spectra of these sources are the result of a chance alignment between a normal C-type giant and one of the many H II regions in NGC 6822, or second, that these sources are Mira variables.

Spectral observations of some of the H II regions in NGC 6822 have shown the Balmer lines and a number of forbidden lines (Peimbert et al. 2005). However, had our spectra been contaminated by an H II region along our line of sight we would expect the lines of [N II] (6548, 6583 Å) to be much stronger. The [N II] 6583 Å line is generally weak in our low excitation emission line sources and the 6548 Å line, which is typically about a third of the strength of the 6583 Å line, is only visible in five cases (ID: 197170, 199754, 200182, 205865, 215861). If our low ionisation emission line sources are plotted on an image of the Hα emission in NGC 6822 we see that they are centrally located (within 1.10 kpc of the galactic centre) and although many of them coincide with diffuse H II regions, so do a number of sources which do not show any emission lines.

Miras represent the terminal phase of the AGB evolutionary track and the presence of Balmer emission lines is often cited as one their their spectroscopic identifiers (Brewer et al. 1996; Richer et al. 1979). The forbidden lines of [S II] and [N II] have also been detected in the spectra of some Miras (Cohen 1980) and are attributed to the shocking of recently ejected material as it encounters the circumstellar envelope (Crowe 1983; Garrison 1997) as such cool stars would not be expected to ionise even low ionisation atoms. Photometrically, Mira variables can be recognised by their photometric variability, but unfortunately, we do not have sufficient photometric data to determine if these sources show such variations. We have therefore cross-matched our sources with a catalogue of variables stars in NGC 6822 published by Battinelli & Demers (2011) and with those sources listed in the recent work of Whitelock et al. (2013).

[1] S has first and second ionisation energies of 10.36 and 23.33 eV. N has first and second ionisation energies of 14.53 and 29.60 eV.

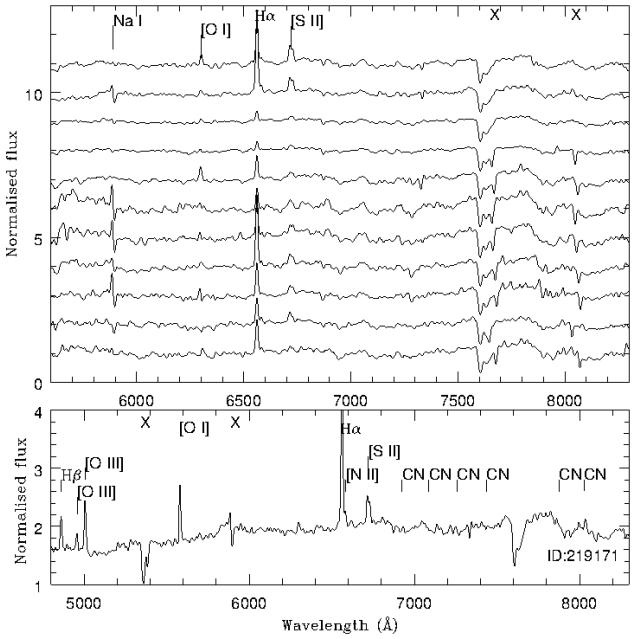

Fig. 10. *Top*: spectra of the 11 inner region high excitation emission line spectra. The spectra are plotted from bottom to top in order of ascending ID number (see Table 4). *Bottom*: spectrum of one of the sources, showing the [O III] and Hβ features. Important molecular and line features have been marked.

We were unable to match any of our low excitation sources with the cyclic, semi- or irregular variables of Battinelli & Demers (2011), but we were able to match two sources (ID: 194777, 213379) with the small amplitude variables listed by Whitelock et al. (2013) in their Table 6. We therefore conclude that these two stars are moving towards the terminal phase of their evolution on the AGB track and the emission lines we see in their spectra are probably the result of shock excitation of material lost from their envelopes. Without further study to determine the variability of the other low excitation sources we cannot confirm if they are also Mira-like stars, but we suggest that this may be the case for the majority of them. However, contamination of the spectra from the H II regions in NGC 6822 cannot be ruled out for those sources showing stronger [N II] emission.

High ionisation sources

Eleven of the emission line sources identified in our sample show lines of [O III] in addition to the molecular features used to identify them as C-type giants. The presence of [O III], which has a second ionising potential (IP) of 35.12 eV, in the spectra of these sources suggests that they are high energy systems.

In the top panel of Fig. 10 we present the spectra for these high ionisation sources. All of the spectra clearly show Hα and the [S II] doublet (the doublet appearing as a single peak at this resolution). [N II] (6583 Å), although present in eight of the sources, is weak in comparison with Hα. The scale of the plot and of the Hα line also make the relatively shallow CN features between 7000–7500 Å difficult to see but the redder features (>8000 Å) are still visible. The spectra have been smoothed in order to be consistent with previous figures. Because of the increasing levels of noise at bluer wavelengths it was decided not to plot all the spectra over the full wavelength range in the top panel, as in some cases the scale of the noise features obscured the features of interest. For this reason we plot the spectrum of only one of the high excitation sources across the full wavelength range in the bottom panel of Fig. 10, so all the main emission features can be seen.

All the spectra show the [O III] 5007 Å line and 10 of them show [O III] 4595 Å, however the [O III] 4363 Å line has not been detected at all, this may be due to the weakness of the line or the low S/N in that part of the spectrum, rather than the absence of the line. Hβ was also detected in nine of the high ionisation sources.

The presence of [O III] requires a hot ionising source in excess of 35 000 K (Gonçalves et al. 2008). These temperatures are more like those of a main sequence O-type star than our AGB targets, however we would not expect to see molecular features in the spectra of such hot objects. Consequently we conclude that our spectra are a composite of at least two objects or systems. We consider two options. First, we again consider the possibility of H II regions in close proximity to our AGB sources. All of our high excitation sources are centrally located, lying within a 0.15 deg^2 region in the centre of the galaxy, and three of them (ID: 173834, 176619, 179746) lie very close to one of the brightest H II regions (V) in NGC 6822. However, another eight high excitation sources lie in regions with only weak Hα emission or in close proximity to sources which show only low ionisation lines or no emission at all. Furthermore, the 6583 Å [N II] line is weak in all of our high excitation sources and we are able to measure the 6548 Å line in only one of the 11 sources. We therefore consider the alternative possibility that some or most of these sources are symbiotic stars.

Symbiotic stars are interacting systems, containing a hot compact source which is accreting material from a cool red giant. In some cases the giant can be a yellow G- or K-type star (yellow symbiotics). Symbiotic systems are subdivided into S- and D-type systems depending on the evolutionary phase of the giant star. Systems that contain a first ascent giant, which is about 80% of systems based on Galactic observations, are classified as S-type, while those sources that contain a Mira variable are referred to as dusty or D-type due to their enhanced mass loss (Belczyński et al. 2000; Phillips 2007). The classification of a system as S- or D-type is usually made based on its NIR colours, as the presence of a Mira variable and emission from dust in the circumstellar shell result in much redder colours for D-type systems (Whitelock & Munari 1992; Corradi et al. 2011). D-type symbiotics are also often associated with an extended ionised nebula formed from material that is not accreted by the hot companion (Corradi et al. 1999, 2011).

Spectrally and physically, symbiotic systems are similar to planetary nebulae (PNe); although they are now treated as a separate class of object owing to the presence of molecular features and a continuum in their spectra. Broadly speaking, symbiotic stars are recognised by the presence of both molecular absorption features and high excitation emission lines in their spectra. More specific criteria for the identification of symbiotics were set by Belczyński et al. (2000), requiring the spectrum to show: 1) the absorption features of a late type giant; 2) strong emission lines of H I and He I and either emission lines of ions with an ionisation potential of at least 35 eV or an A- or F-type continuum with additional absorption lines; and/or 3) an emission feature at 6825 Å even if no features of the cool star are seen. The broad feature at 6825 Å and a second at 7082 Å, which result from the Raman scattering of O VI photons by neutral hydrogen (Schmid 1989), have until recently only been seen in the spectra of symbiotic stars, and are commonly used as conclusive evidence of the symbiotic nature of a system. However, Leedjärv et al. (2004) note that half of the symbiotic stars in the catalogue

Table 4. 11 inner region (top) and 4 (bottom) outer region sources that show the high excitation emission lines of [O III].

ID	RA (2000.0) (deg)	Dec (2000.0) (deg)	J (mag)	H (mag)	K (mag)	Phot. type	Dist. (kpc)	Spec. type	Kmatch	Dmatch	Letarte ID	$R-I$ (mag)	CN–TiO (mag)	S/N
173834	296.22287	–14.71018	17.60	16.76	16.37	C*	0.80	Ce	C	C	390.0	1.338	0.503	12
176619	296.22888	–14.72012	17.50	16.56	16.30	M	0.71	Ce	C3.2	C	431.0	1.316	0.405	14
179746	296.22033	–14.72841	18.26	17.25	17.15	M	0.65	Ce	C3.2	S	370.0	1.265	0.404	11
181364	296.12738	–14.73369	17.56	16.81	16.41	M	1.09	Ce	C8.2e	C	96.0	1.171	0.311	12
182253	296.31088	–14.73645	17.18	16.31	15.91	C*	0.83	Ce	C	C	769.0	1.226	0.661	11
183545	296.28564	–14.74075	16.67	15.62	15.09	C*	0.67	Ce:	C5.5	C	701.0	1.577	0.509	12
194386	296.18609	–14.77870	16.72	15.90	15.54	M	0.47	Ce	C	C	228.0	1.337	0.472	19
196632	296.24578	–14.78650	17.58	16.73	16.46	M	0.16	Ce:	dK7	K0III	513.0	1.179	0.399	23
199930	296.23651	–14.79789	17.25	16.52	16.22	M	0.05	Ce	dK7	K0III	474.0	1.148	0.475	31
219171	296.22512	–14.86821	17.31	16.58	16.32	M	0.57	Ce	C8.2e	K0III	407.0	1.122	0.403	11
220391	296.21267	–14.87307	17.66	16.80	16.47	M	0.63	Ce	C	C	328.0	1.156	0.59	13
22972	295.98809	–13.95111	18.11	17.36	17.12	M	7.57	dMe:	dM0	M0V	–	–	–	10
30076	295.96771	–13.98843	17.87	17.09	16.91	M	7.32	dMe	dM0	M0V	–	–	–	14
76159	295.95544	–14.21816	18.09	17.36	17.22	M	5.52	dMe:	dM1.5	M0V	–	–	–	11
87125	295.95578	–14.27512	18.01	17.29	17.19	M	5.08	Uncl	dK7	K3III	–	–	–	12

of Belczyński et al. (2000) do not show this feature. Therefore, although the presence of the Raman features are a strong indicator that a star is symbiotic, their absence does not exclude the possibility. The presence of ionisation conditions that are sufficient to produce lines of He II (4686 Å) is another commonly used criterion, attributed to Allen (1984).

The presence of molecular features and emission lines in the spectrum of our high ionisation sources agrees well with the broad spectral description of symbiotic stars. However, the absence of the Raman features (which we would expect to see in ∼50% of our suspect symbiotics) and the high ionisation He II line[2] at 4686 Å might suggest otherwise. On the other hand non-detection of the Raman features is not conclusive, and the relative weakness of the features, as seen in other symbiotics (Kniazev et al. 2009; Gonçalves et al. 2008), means that if present they may have been lost in the noise of the spectrum. The problem of noise worsens at bluer wavelengths and may also account for the non-detection of He II. Neither of these features are detected in the spectrum of the suspected symbiotic in IC 10, IC10 SySt-1 (Gonçalves et al. 2008).

The spectra of the three sources that lie close to the H II region (V) could be the result of a chance alignment or they may be symbiotic in nature. Of the eight high ionisation sources that do not lie near a bright H II region, if they are symbiotic stars, the weakness of the [N II] lines suggests that these sources are S-type, as [N II] emission is typically much stronger in D-type symbiotics (Corradi et al. 2010, 1999). This preliminary classification is supported by the position of these sources in the ($H-K$, $J-H)_0$ colour–colour diagram in the bottom panel of Fig. 11, when compared with the same diagram of S- and D-type symbiotics presented by Whitelock & Munari (1992). The majority of our high ionisation sources have $(H-K)_0$ colours that are slightly redder than the locus of S-type symbiotics but they lie close to NGC 6822 SySt-1 – the only previously known symbiotic star in NGC 6822 (Kniazev et al. 2009) – which is also shown in Fig. 11 and was classified as an S-type system using the same diagram. Kniazev et al. (2009) attribute the redder colours of NGC 6822 SySt-1 to the presence of a carbon giant in the system, which is also consistent with our sources.

The identification of one known and eight potential symbiotic stars all containing C-type stars is surprising given that carbon rich symbiotics are rare in the MW (Corradi et al. 2011). This is probably a reflection of the lower metallicity and higher fraction of C-type stars in NGC 6822. However, this is where the similarities between our potential symbiotics and NGC 6822 SySt-1 end. Unlike our sources, the spectrum of NGC 6822 SySt-1 shows the 6825 Å Raman feature and excitation lines of He I and He II but does not show the molecular features of the giant. The absence of the molecular features is not unknown in the spectra of symbiotic stars which have a lot of cool dust emission (Phillips 2007); but Kniazev et al. (2009) attribute the lack of these features to the low level of signal in the continuum. Comparing the spectra of our sources with other known symbiotic stars in the Local Group, we find the greatest similarity, aside from the strength of the [N II] lines, with the spectrum of the suspected D-type symbiotic IC10 SySt-1 (Gonçalves et al. 2008).

In order to try to establish a clearer classification for our high ionisation sources, emission line fluxes were measured to estimate the relative strengths of the lines and permit calculations of the electron densities (N_e) and temperatures (T_e). Using IRAF a Gaussian profile was fitted to the visible Balmer, [N II], [S II] and [O III] lines to measure the flux. The stsdas routine temden (Shaw & Dufour 1994) was then used to estimate N_e and to constrain T_e in the environments around the individual sources using the ratios [S II] $I(6717)/I(6732)$ and [O III] $I(5007+4959)/I(4363)$ respectively (Osterbrock 1988). The values derived for N_e and T_e are presented in Table 5. Where possible these values have then been compared to those for the two brightest H II regions in NGC 6822, NGC 6822 SySt -1 and the IC10 SySt-1 to establish any similarities between these environments and those around our high excitation sources.

For our high excitation sources we derive N_e values of $\sim 10^2$ cm^{-3}, excluding source ID: 220391 for which we were unable to derive a value of N_e. Higher densities are expected for the regions around S-type symbiotics and Kniazev et al. (2009) estimate a maximum value of 10^9 cm^{-3} for NGC 6822 SySt -1 given the absence of forbidden line emission. Our N_e values are more consistent with the value derived for IC 10 SySt-1 by Gonçalves et al. (2008), who estimate a value of 400 ± 200 cm^{-3} using the [S II] ratio. Given the low density, Gonçalves et al. (2008) suggested that these lines may originate in an extended nebula which would be consistent with the suspected

[2] He has a first ionising potential of 24.59 eV.

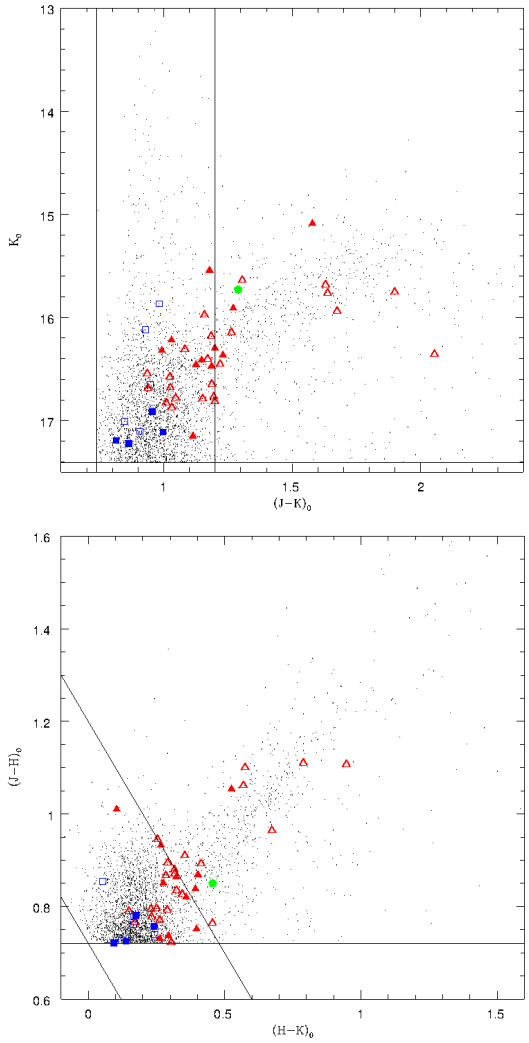

Fig. 11. *Top*: high (solid shapes) and low ionisation (open shapes) sources from the inner (red triangles) and outer (blue squares) regions are plotted on a CMD of the AGB sources from Paper I. The horizontal and vertical lines mark the selection criteria used in that paper. The green pentagon marks the position of NGC 6822 SySt 1 (Kniazev et al. 2009). *Bottom*: same sources plotted on a $(H-K, J-H)_0$ colour–colour diagram. The horizontal and diagonal lines mark the selection criteria used in Paper I.

D-type nature of this object. However, similarly low N_e values of 10^1–10^2 cm^{-3} are derived by Peimbert et al. (2005) for the two large H II regions, V and X, in NGC 6822. The similar densities in the two types of system mean that we cannot differentiate between them based on our derived values of N_e.

As the [O III] 4363 Å line is not visible in our spectra we were not able to measure its flux directly in order to estimate T_e. We have therefore derived a maximum value for this line based on the assumption that it is present but is not visible above the level of the noise in that part of the spectrum[3]. This has enabled us to put an upper limit on the electron temperature, however, our estimated values and therefore our derived ratios are strongly affected by the low S/N at wavelengths <4800 Å. Although higher

[3] This maximum value has been calculated as three times the typical noise level (σ) in the blue part of the spectrum, where σ has been calculated as $\sqrt{2N_{\rm pix}X}$. $N_{\rm pix}$ is the FWHM in pixels of the weakest line we were able to measure (usually H_β) and X is the estimated level of the continuum at 4363 Å divided by the S/N between 4430 and 4570 Å.

Table 5. Estimates of N_e and T_e for the same sources as in Table 4 are shown in the top and middle sections.

ID	N_e (cm^{-3})	T_e (K)
173 834	189	>70 000
176 619	442	<66 800
179 746	357	<69 800
181 364	475	>70 000
182 253	205	>70 000
183 545	298	<27 400
194 386	486	>70 000
196 632	874	>70 000
199 930	364	>70 000
219 171	410	>70 000
220 391	–	–
22 972	528	–
30 076	1320	–
76 159	2290	<64 600
87 125	315	–
NGC 6822 SySt-1	<10^9	–
IC 10 SySt-1	400 ± 200	<17 000
H V	90–190	11 900–15 500
H X	30–100	12 000–13 300

Notes. In the bottom section we have listed the electron density and temperature measurements for two symbiotic stars and two H II regions for comparison.

electron temperatures may be expected in NGC 6822, compared to the MW for example, due to its lower metallicity, the upper limits we derive are significantly higher than the T_e estimates made for the two brightest H II regions in NGC 6822 and that derived for IC 10 SySt-1 (~17 000 K). Given that we derive N_e values similar to those of IC10 SySt-1 we would have expected similar values of T_e. The difference in the derived values suggests that our [O III] ratio can only be used as a very rough guide to the electron temperature and therefore we will not attempt to draw any further conclusions about our emission line sources based on it.

We have speculated about two possible causes for the presence of the high energy forbidden lines in the spectra of 11 of our inner region sources, however we are cautious in assigning a definite cause. While contaminating emission from H II regions in NGC 6822 may be the most plausible explanation for our high excitation sources, the high temperatures required to produce emission lines of [O III] suggest that these regions would have to contain hot, bright O-type stars and should be clearly visible in the vicinity of our targets, however this is the case for only three of our high ionisation sources. On the other hand while the emission line and molecular features seen in the spectra of these sources are compatible with the broad definition of symbiotic stars, the detection of such a large number of these unusual objects would need to be explained. Further observations are clearly necessary before any of these sources can be classified with certainty.

While these sources, high and low ionisation, have provided an interesting addition to our main sample, they are not the main focus of this work and their emission line characteristics will not be discussed further. They will however, be included in the statistics we present in later sections, as regardless of the emission lines seen in their spectra, they are C-type giant stars and

are therefore relevant to the discussion of how well such stars are selected using optical and *JHK* photometry.

4.1.3. Unclassified sources

Of the 85 sources in the inner region for which we have obtained spectra we have been unable to classify two (ID: 186430 and ID: 233186). In Paper I the first of these was classified as an M-type giant while the second was excluded from the main sample due to its flag classifications and was not classified. Both sources were classified as C-type by Letarte et al. (2002) and as K-type dwarfs (dK7) by the automated matching program used here. The spectra of these two sources are shown in Fig. 12. It can be seen clearly that both sources show very shallow absorption features redward of ∼7800 Å that are similar to those of the CN bands at 7879 Å and 8026 Å in C-type stars. The presence of these features probably resulted in their being present in the catalogue of Letarte et al. (2002), however, neither source shows the more recognisable CN features at 6925, 7088, 7259 and 7437 Å. Both spectra are relatively featureless in regions 1 and 2 and are not dissimilar to the average dK7 spectrum, however the very weak Na D lines and the lack of any other recognisable features mean that we are not confident in classifying these sources as K-type dwarfs.

An examination of the *JHK* colours of source ID: 186430, $(J-K)_0 = 0.99$ mag, $(J-H)_0 = 0.77$ mag and $K_0 = 16.24$ mag, show that in the CMDs and colour–colour diagrams of Fig. 9 it sits in the transition region between the spectroscopically confirmed dwarf and C-type giant sources and so cannot be classified reliably using photometric colours. Using the derived colour ratios (Sect. 3.1.3) for this source it is classified as a foreground dwarf, but for all three ratios the source is located very close to the boundaries we impose between the giant and dwarf sources (see Fig. 5).

With regards to source ID: 233186, as no *J*-band magnitude for this source was recorded we are unable to draw any conclusions about its nature based on either its *JHK* photometry or its derived colour ratios. However, we note that the presence of Hα in absorption suggests that this star is hotter than we would expect for a K-type dwarf source.

We have been unable to classify these sources and so have listed them as unclassified in Table 10. As they have not been identified as C-type stars they will not be considered among the candidates successfully classified by Letarte et al. (2002) when we consider the success of the CN–TiO method.

4.1.4. *JHK* vs. CN–TiO method

We now compare the photometric classifications assigned to our spectral sources using the CN–TiO method and *JHK* photometry, to assess which method was most successful. However, the lack of M-type giants in our spectroscopic sample and the lack of M-type candidates in the catalogue of Letarte et al. (2002) means that we limit this discussion to the identification of C-type AGB stars.

All of the 85 spectroscopic targets in the inner region were classified as C-type giants by Letarte et al. (2002) and the majority (78 sources or 93%) have been confirmed as such. On the other hand, for classifications assigned using the *JHK* criteria developed in Paper I the success rate is much lower (28%) as can be seen in Table 3. For the 58 cases where the *JHK* criteria of Paper I and the CN–TiO criteria of Letarte et al. gave differing classifications the CN–TiO classification prevailed in 54 cases. If

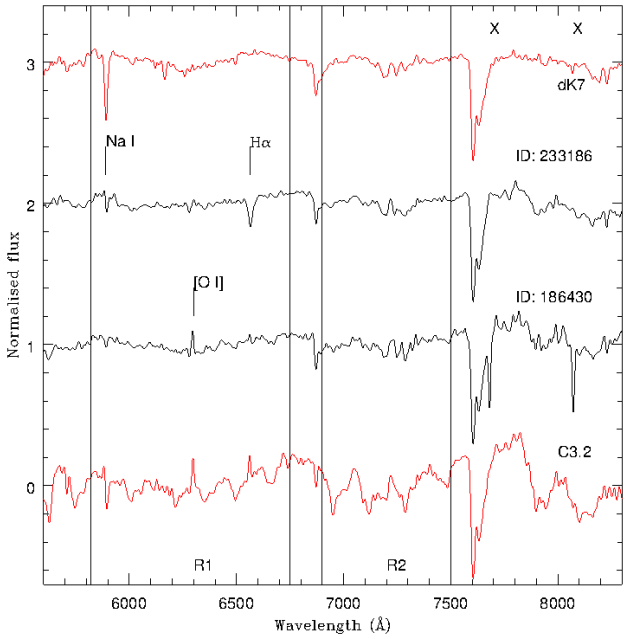

Fig. 12. Spectra of the two unclassified sources in the inner region (solid black lines). At the bottom we have plotted the average C3.2 spectrum and at the top we have plotted the average dK7 spectrum (solid red lines) for comparison. The crosses mark the positions of spurious features (Sect. 2.2).

the 32 low S/N sources at $r \leq 3$ kpc are examined (Table 12), we see that Letarte et al. have again classified 93% of the sources correctly compared to only 37% when using the *JHK* criteria. Half of the 30 C-type stars in this lower quality sample were misclassified as M-type giants using the *JHK* classifications. These comparisons make it clear that the *JHK* criteria presented in Paper I misclassify a fraction of genuine C-type stars as M-type stars and show that the CN–TiO method has, overall, been the more reliable method.

The success of the CN–TiO method within our sample is consistent with previous work (Battinelli & Demers 2005; Groenewegen 2006) and is not too surprising given the use of narrow band photometry. However, the presence of eight non C-type sources (four dK, one dM, one M-type giant and two unclassified) among this subset of 117 Letarte et al. (2002) sources, if the lower quality sample is included, shows that the CN–TiO method is still susceptible to contamination at the ∼7% level.

The presence of an M-type dwarf (ID: 173114, see Fig. 13) among the contaminants is most puzzling as the narrow band filters should have excluded it due to the strength of its TiO bands. We considered the possibility that the spectra we obtained were not of our intended target, but the closest neighbour to the dM source is ∼2.7″, while the fibres of the spectrograph have radius of only 1.05”. It is unlikely that a fibre placed on our chosen target would detect light from this object. The presence of an M-type giant in this subset of Letarte et al. (2002) sources is attributed to the anomalous CN bands seen in the spectrum of this particular source (Sect. 4.1).

Assuming then that the spectra we have obtained are those of our intended targets, we examine the $(R-I)$ and (CN–TiO) colours of these misclassified sources. The M-type giant source (ID: 197590) has an $(R-I)$ colour of 1.48 mag, which is consistent with both C- and M-type stars according to Letarte et al. (2002) but its (CN–TiO) = 0.61 mag value places it well within the C-type star box of Letarte et al. (2002). The dM

Table 6. Summary of the classifications assigned in this work, and in Paper I, to the 77 sources in our spectral sample for the outer region.

Spec. type	Phot. type (Paper I)				
	M-type giant	C-type giant	RGB	Foreground	Excluded
M-type giant	0	0	0	0	0
C-type giant	2	1	0	0	0
M-type dwarf	48	1	0	0	0
K-type dwarf	22	1	0	0	0
Unclassified	1	1	0	0	0

Notes. The column headed as excluded refers to those sources that were excluded in Paper I due to the quality flag criterion used.

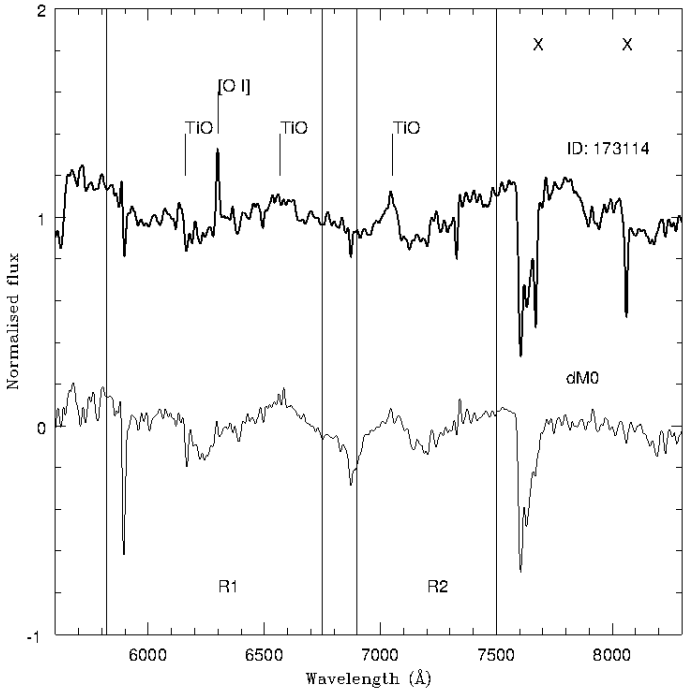

Fig. 13. Spectrum of source ID: 173114 (bold line), ID: 799 in the catalogue of Letarte et al. (2002). This star was classified as C-type using the CN–TiO method but has been spectroscopically classified as an M-type dwarf in this work. Below is plotted the average dM0 spectrum for comparison. The TiO bandheads and other molecular and atomic features have been marked.

source has $(R - I)$ and (CN–TiO) colours of 1.28 and 0.42 mag respectively, similar to those of the dK sources in the inner region, which have colours in the range $(R - I) = 1.11–1.25$ and (CN–TiO) = 0.33–0.45. This places all the dwarf sources of the inner region in the bottom left-hand corner of the C-type selection box outlined by Letarte et al. (2002). The localised distribution of these sources near the edge of the selection area suggests that the selection criterion of Letarte et al. (2002) needs to be tightened.

4.2. Outer region sources

Of the 77 sources in the outer region for which we collected sufficiently high quality spectral data, 75 have been classified. The majority of these sources have been classified as foreground dwarf stars (49 M-type and 23 K-type), a further three have been classified as C-type giant stars, and two more remain unclassified. A summary of these spectral classifications, as well as the photometric classifications assigned to these sources in Paper I, is shown in Table 6.

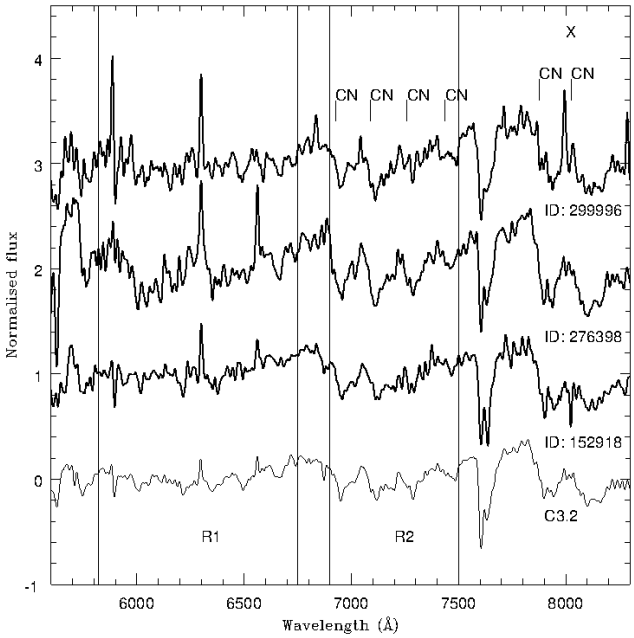

Fig. 14. Spectra of the three C-type stars identified in the outer region (thick black lines). For comparison we have plotted the average C3.2 spectrum at the bottom (thin black line).

4.2.1. *JHK* photometric colours

In the two right hand panels of Fig. 9 we present a CMD and a colour–colour diagram of the spectroscopically classified sources in the outer region. Three of these are C-type stars, the spectra of which can be seen in Fig. 14, while the remainder are foreground dwarf stars. The dwarf sources exhibit a much narrower range of $(J - K)_0$ and $(J - H)_0$ colours compared to the C-type giant population overall. The $(J-K)_0$ colours of the three C-type sources in the outer region fall in the middle of the colour range for sources of the same type in the inner region.

The M-type dwarf sources occupy a colour range between $(J - K)_0 = 0.83–1.04$ mag, with a peak in the colour distribution between $(J - K)_0 = 0.9–1.0$ mag. These findings are broadly consistent with those of Kacharov et al. (2012) who found that the majority of M-type dwarf sources in their sample lay between $(J - K)_0 = 0.7–1.0$ mag, peaking at slightly bluer colours, $(J - K)_0 = 0.80$ mag. The K-type dwarf population, excluding one very red outlier (ID: 63349), lies in the range $(J - K)_0 = 0.75–1.17$ mag, and peaks around $(J - K)_0 = 0.80–0.90$ mag.

We now consider the $(J - H)_0$ colours of the dwarf population. The majority of both the K- and M-type dwarf populations lie at $(J - H)_0 < 0.80$ mag; the M-type dwarf sources cover a range of $(J - H)_0 = 0.72$ to 0.95 mag, with a peak

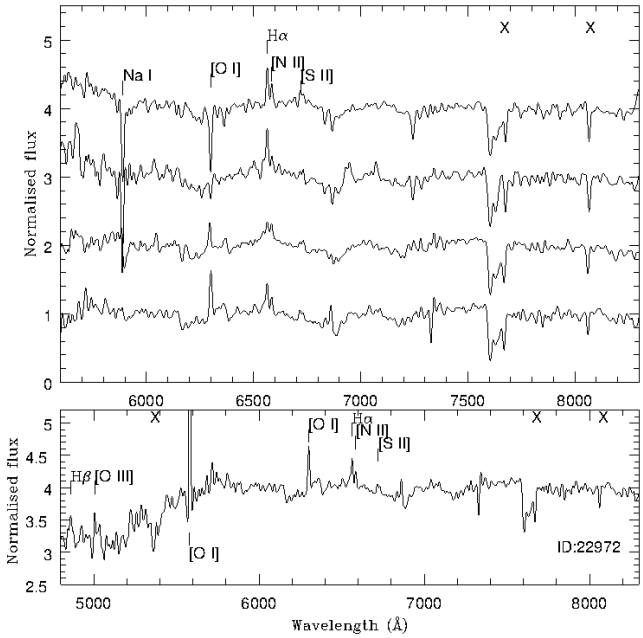

Fig. 15. *Top*: the four high ionisation emission line spectra in the outer region. The spectra are plotted from bottom to top in order of ascending ID number (see Table 4). *Bottom*: spectrum of one of the above sources, showing the [O III] and Hβ features. Important emission line features have been marked.

in distribution around 0.74 mag, while the K-type dwarfs have $(J-H)_0$ colours between 0.72 and 0.99 mag and the distribution peaks around 0.76 mag.

The number of dwarf sources in our spectroscopic sample lying between $0.72 < (J-H)_0 < 0.80$ mag clearly has implications for the *JHK* selection criteria derived in Paper I and will be discussed further in Sect. 5.1.3. Importantly, the clustering of these K- and M-type dwarf stars at values of $(J-H)_0 < 0.80$ mag, where foreground dwarfs are expected (see extensive discussion in Paper I) provides photometric confirmation that the spectroscopic classification of these stars as K- and M-type dwarfs, is correct.

4.2.2. Emission line stars

Nine sources in the outer region were found to show Hα in emission. Five of these sources also showed the forbidden lines of the [S II] and in some cases [N II] (6583 Å), while four showed both of these lines, the 5007 Å line of [O III] and in some cases Hβ. All of the outer region emission line sources were classified as M-type dwarfs, with the exception of source ID: 87125 which is unclassified but which we believe to be a dwarf star (see Sect. 4.2.3). Those sources which show the low excitation emission lines are denoted by an e in their classification in Table 11, while those sources that show the higher excitation [O III] line in emission are listed separately in the lower part of Table 4. We include source ID: 206129 in our discussion of the outer region low excitation sources as although it was detected among our inner region sources it has been classified as a K-type dwarf and is therefore thought to be a foreground contaminant like the outer region sources.

In the top panel of Fig. 15 we present the spectra of the four high excitation sources in the outer region. As in Fig. 10 we have restricted the wavelength range in the top panel because of increasing noise at bluer wavelengths and present the spectrum of only one of the high excitation sources (ID: 22972) over the wider wavelength range of 4800–8300 Å in order to show the presence of the forbidden lines of [O III] and Hβ.

Balmer emission lines have previously been detected in late K-type dwarfs with enhanced chromospheric activity and their presence becomes increasingly common with later spectral type through to late-M (Hawley et al. 1996). We consider the possibility that the dwarf emission line sources we detected are flare stars, also called active red dwarfs. However, although the high excitation emission lines of He II have also been detected in such stars, forbidden lines are not typically seen (Gurzadyan 1977). Based on work by Corradi et al. (2008), we considered the possibility that these sources are T-Tauri stars. As part of their ongoing study to characterise the colours of symbiotic stars in the IPHAS and 2MASS catalogues, Corradi et al. (2008) plotted a $(H-K, J-H)_0$ colour–colour diagram showing the positions of common symbiotic mimics. From that plot it is clear that T-Tauri stars follow a track which is parallel to that of C-type AGB and S-type symbiotic stars. It is therefore plausible based on the colour selection used in Paper I that such sources may be among the foreground interlopers included in the photometric AGB catalogue. Spectra of these pre-main sequence objects show both molecular features and the forbidden lines, including [O III], that we see in our spectra (Looper et al. 2010; Joergens et al. 2012). The visibility of the [N II] 6548 Å line in the spectra of our outer region sources is suggestive of a more nebulous environment which would also be appropriate. Both the high and low excitation sources in the outer region as well as sources ID: 206129 are presented on the CMD and colour–colour diagram presented in Fig. 11. However, as our line of sight to NGC 6822 does not pass through any star forming regions that we are aware of, it would be very unusual for such a large number of Galactic T-Tauri stars to be included in our observations. Alternatively, perhaps our observations of these sources have been contaminated by emission from the interstellar medium (ISM) in NGC 6822, although this would be beyond the 4 kpc radial limit, or from the Galactic ISM along the line of sight.

We are unable at this time to draw any conclusions about the exact nature of the emission line sources in the outer region. However, given the consistent presence of the [S II] doublet in all of the high excitation sources we have calculated N_e, and using the same technique described in Sect. 4.1.2, we have estimated the maximum strength of [O III] 4363 Å for those sources that showed the 4959 Å line, in order to provide a maximum for T_e. These values are presented in the lower part of Table 5.

4.2.3. Unclassified sources

We have been unable to classify two sources in the outer region (ID: 87125, 346806). In Paper I the first of these sources was classified as an M-type giant star and the second was classified as a C-type giant star, while both were classified as dK7 by the automated matching program. Neither spectrum shows any obvious molecular features which we can use to classify them, however both show other unusual elements.

The H Balmer and forbidden emission lines seen in source ID: 87125 have already been discussed in Sect. 4.2.2. The spectrum of this source also shows the presence of an absorption feature at 7245 Å that we have been unable to identify. However, as strong absorption features at the approximate location of the [O I] 6300 and 6363 Å lines are also seen in this spectrum, probably resulting from an over subtraction of night sky emission lines, the feature at 7245 Å may be an artifact resulting from

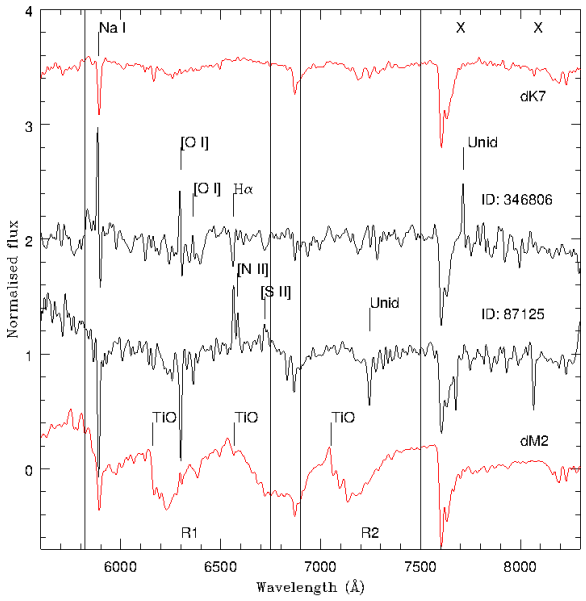

Fig. 16. Spectra of the two unclassified sources in the outer region (solid black lines). At the bottom we have plotted the average dM2 spectrum and at the top we have plotted the average dK7 spectrum (solid red lines). Important molecular and line features have been marked.

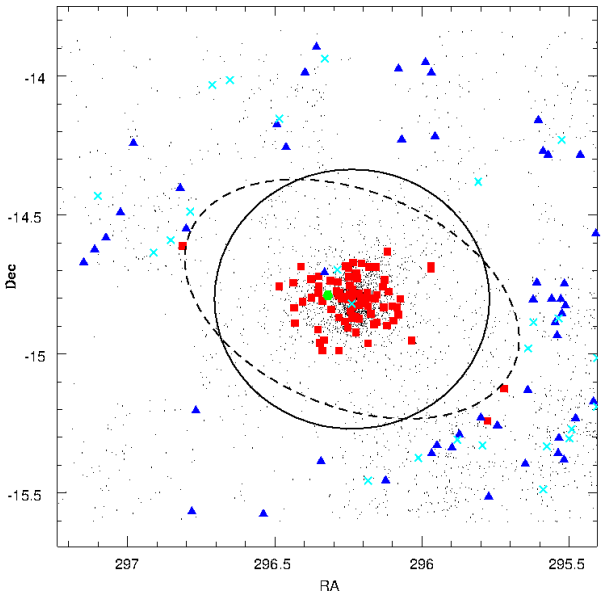

Fig. 17. Distribution of all the candidate AGB sources (black dots) identified in Paper I. Overlayed are sources from our spectroscopic sample. Symbols have the same meaning as in Fig. 5. The circle (solid line) marks the position of the 4 kpc limit inferred in Paper I. The ellipse of Battinelli et al. (2006, dashed line) is shown and has a semi-major axis of 34′ at the assumed distance modulus assumed in Paper I, $(m - M)_0 = 23.45 \pm 0.05$.

imperfect sky subtraction. The *JHK* colours and magnitudes for this source are $(J - K)_0 = 0.81$ mag, $(J - H)_0 = 0.72$ mag and $K_0 = 17.19$ mag and place it among the dwarf sources in the CMD in Fig. 9 as do the derived colour ratios (Sect. 3.1.3) for this source. A dwarf classification is also supported by the strong Na D line we see in its spectrum which is presented in Fig. 16, but again, this may be affected by an over subtraction of night sky emission lines.

The *JHK* photometry for source ID: 346806 places it with the C-type giant sources (Fig. 9) and tentative support is provided for a giant classification by two of the three derived colour ratios, although the source does sit close to the transition region between the dwarf and giant sources in all cases (Fig. 5). The presence of Hα in absorption suggests that the source is hotter than we would expect for a dwarf star. Finally, we note the presence of an unidentified emission line at 7713 Å which is not seen in any of our other spectra. However, the clearly visible 6300 and 6363 Å ([O I]) emission lines show that the removal of night sky features from the spectrum is incomplete and the feature at 7713 Å maybe a relic of that imperfect process.

We have been unable to provide a spectral type for these sources and have therefore listed them as unclassified in Table 11. We present the spectra of these two objects in Fig. 16 and for comparison we also show the average dM2 and dK7 spectra.

4.3. The structure of NGC 6822

In Paper I it was concluded that the majority of the AGB sources in NGC 6822 lay within a radial distance of 4 kpc from the galactic centre and that beyond this limit AGB sources could not be reliably disentangled from the contaminating MW foreground.

The distribution of spectral types in the inner and outer regions is in good agreement with this conclusion.

4.3.1. The extent of the galaxy

An examination of the spatial distribution (Fig. 17) of our spectroscopically confirmed C-type star population shows that of the 82 C-type stars we identify, all but three lie within 3 kpc of the galactic centre. Of the C-type stars identified in the outer region, none lies further than ∼5.5 kpc from the galactic centre (see Table 11), on the periphery of the elliptical outer structure of NGC 6822 described by Battinelli et al. (2006) (sometimes referred to as the spheroid) which extends to a distance of ∼5.0 kpc along its semi-major axis. This structure is outlined in Fig. 17. Given the alignment of the C-type sources with the long axis of the spheroid we believe they are probably part of this structure. From our limited sample we cannot determine how far the elliptical structure extends, but Battinelli et al. (2006) find that a non-negligible number of C-type stars are detected up to a distance of 40′ (∼5.5 kpc). Based on our density profile analysis in Paper I and the low number of spectroscopically confirmed AGB sources detected beyond 5 kpc, we suggest that the number of genuine NGC 6822 AGB sources declines rapidly in the outer portions of the galaxy and that 40′ may be an upper limit for the semi-major axis of the spheroid. This echos the findings of Kacharov et al. (2012) who, despite having a larger spectroscopic sample than ourselves did not detect any AGB sources beyond the elliptical structure of Battinelli et al. (2006).

Of the 77 sources in the outer region for which we have sufficiently high quality spectra, 72 have been classified as K- or M-type dwarfs, i.e. foreground objects, which seems to strongly support conclusions drawn about source density in Paper I.

The selection of targets (Sect. 2.1) in the outer region included 178 M-type and 10 C-type giant stars, according to their photometric classifications. A bias towards the selection of M-type sources for spectroscopic follow-up in the outer region was a minor concern. However, given that the $(J - K)_0$ colour distribution (Sect. 4.1.1) of the confirmed C-type sources

Table 7. Number of sources from the photometric catalogues of Paper I that were matched with sources in the catalogues produced by the authors listed in the left hand column.

Reference	AGB (≤4 kpc)	AGB (>4 kpc)	RGB	Foreground	Excluded
Letarte et al. (2002)	635	0	0	0	235
Kang et al. (2006)	294	0	0	63	266
Demers et al. (2006)	78	0	0	0	51
Battinelli & Demers (2011)	12 (17)	0 (0)	0 (0)	3 (1)	14 (9)
Kacharov et al. (2012)	273	13	1	219	34
Whitelock et al. (2013)	26 (60)	0	0	5 (5)	21 (20)

Notes. The classification assigned to these sources in Paper I is given in the column headers. Those listed as excluded were rejected from the photometric sample due to the three band flag criterion of Paper I. For Battinelli & Demers (2011) the numbers given in brackets refer to the number of matches with the semi-regular or irregular LPVs, those not in brackets are the number of matches with their regular LPV sources. For Whitelock et al. (2013) we give the number of sources matched with their small or large amplitude variables with no determined period in brackets, numbers not in brackets refer to sources matched with their list of C- or M-type Mira.

extends significantly blueward of the colour boundary applied in Paper I, many of the sources photometrically classified as M-type giants could in principle have been C-type stars, resulting in many more than 10 C-type candidates being included in the spectral sample. The fact that only three such stars are identified is then even more significant. We conclude that the paucity of C-type AGB sources beyond 5 kpc is real and declines between 3 and 5 kpc. The lack of M-type giant sources is equally significant, as we would expect them to be more numerous than the C-type stars. We therefore conclude that although the radial limit at 4 kpc imposed in Paper I was conservative, it was reasonable. Had the limit been extended to between 5.0–5.5 kpc, it would have resulted in significantly higher levels of foreground contamination for relatively little return. Based on the $(J-K)_0$ colour distributions of the K- and M-type dwarfs in our spectroscopic sample (Sect. 4.2.1) it is also likely that the majority of the foreground interlopers would have been classified photometrically as M-type sources and would have skewed both the C/M ratio and the iron abundance derived from it.

4.3.2. The SW overdensity

Surface density plots for the C- and M-type AGB and RGB candidates and the foreground sources were presented in Paper I (their Fig. 11). The M-type AGB sources showed a clear overdensity in the south-west (SW) that was not seen in the other plots and it was noted that if the overdensity in the SW was a real feature it appeared to be populated almost entirely by M-type AGB stars. However, given the bluer $(J-K)_0$ colour distribution of our spectroscopically confirmed C-type sample (Sect. 4.1.1), if the sources in the SW are genuine AGB stars belonging to NGC 6822, then a significant number may actually be C-type stars. Kacharov et al. (2012) also found, based on the same photometric data and their own selection criteria, that the highest number of probable galactic sources outside the elliptical structure of Battinelli et al. (2006) was in the SW and that the majority of these were classified as M-type giants.

In Paper I we queried whether the SW overdensity was the result of excess leakage of foreground sources into the AGB candidate sample. This interpretation is now more strongly supported as our spectroscopic work does not detect any M-type AGB stars and only two C-type stars, in the vicinity of the overdensity. It therefore seems likely that the SW overdensity is not a real feature, but the result of excess foreground contamination in this region. Arguments are presented in Paper I as to why such an overdensity is seen only in the SW, and we refer the reader to that paper.

5. Discussion

5.1. Revisiting the Paper I selection criteria

5.1.1. The *JHK* method

We established in Sect. 4.1.4 that based on our spectroscopic sample, the CN–TiO method has been the more reliable for the selection of C-type AGB stars. We now examine the comparatively low success rate of the *JHK* method and if this is solely the result of poor selection criteria or if the way in which the spectroscopic targets were chosen has had an adverse effect on our results.

All of the photometric candidates in the inner region for which spectra were obtained were selected to be in common with the catalogue of C-type stars presented by Letarte et al. (2002); this was done to allow us to estimate the level of agreement between the *JHK* and CN–TiO methods. Unfortunately it also means that the stars for which we have gathered spectra are not representative of the *JHK* selection criteria alone, and hence we cannot infer an unbiased misclassification rate for the *JHK* method from these statistics. In particular by selecting sources with opposing classifications to those we assigned in Paper I we have effectively selected a subsample of the *JHK* classified population with the highest probability of errors.

In the outer region, targets were selected without reference to any other data, but two of the three sources spectroscopically classified as C-type giants were photometrically classified as M-type stars. This suggests that rates of misclassification among the photometric M-type sources may be high. We are unable to comment on the number of M-type giants that are likely to be misclassified as C-type sources.

5.1.2. Photometric flag criterion

To ensure that only the best quality photometry was used for the determination of the *JHK* selection criteria, strict quality control criteria were applied in Paper I. From the raw *JHK* photometric catalogue of ~375 000 sources, only those flagged as stellar or probably-stellar in all three bands were considered, reducing the sample to ~150 000 sources which were then classified as AGB, RGB or foreground. However, after cross matching our catalogues with those of Kang et al. (2006) and Letarte et al. (2002), on the basis of their astrometry, it was found that a significant

number of the matched sources (see Table 7) were found among those sources that had been rejected due to the lower quality of their photometry. This pattern was repeated when further cross-matching was undertaken using recently published catalogues (Battinelli & Demers 2011; Kacharov et al. 2012; Whitelock et al. 2013), this suggests that the quality control measures applied in Paper I were too stringent. In order to investigate this issue, a number of the originally excluded sources that were matched with a source in the catalogue of Letarte et al. (2002) were included in our list of spectroscopic targets for the inner region; 56 such sources were observed, 35 with $S/N \geq 10$ and 21 with $S/N < 10$. These originally excluded sources are marked by a * in the sixth column of Tables 10 and 12.

Of these 56 sources, we have been able to classify 50 as C-type giants, four are classified as K- or M-type dwarfs, one is an M-type giant and one is unclassified. This confirms that a number of genuine AGB sources were removed from the photometric sample presented in Catalogue 1 of Paper I. However, 60% of the 51 AGB sources were retained in Catalogue 3 of the same paper, which contains sources classed as stellar or probably-stellar in two or three photometric bands.

Given these findings, we re-evaluate our original photometric data and apply the selection criteria determined in Paper I to all the sources of Catalogue 3. This results in 6278 candidate C- and M-type AGB sources across the full photometric observing area, ~2500 more than were found in the same area using the three flag criterion in Paper I. Within the 4 kpc limit, the increase in the number of photometric AGB sources is not quite as dramatic, but the greater number of these sources are classified as C-type stars.

5.1.3. Foreground contamination

The low Galactic latitude of NGC 6822 ($l = 25°.34$, $b = -18°.39$) meant that our photometric observations suffered from heavy foreground contamination. Based on the work of Bessell & Brett (1988) and on the distribution of the sources in $(H-K, J-H)_0$ space, a colour cut at $(J-H)_0 = 0.72$ was used to remove foreground dwarfs (and K-type giants) from Catalogue 1 in Paper I. This colour cut was consistent with the intrinsic colour range Bessell & Brett (1988) found for M-type dwarfs ($(J-H) \leq 0.69$ mag) and giants ($(J-H) \geq 0.83$ mag), but will also have included the K4 and K5 giants ($(J-H) \geq 0.73$ mag) in our sample. Using our spectroscopic sample we now assess how successful our $(J-H)_0$ colour criterion was at separating the foreground and extragalactic populations.

Of the 158 sources that we have been able to classify in our main ($S/N \geq 10$) spectroscopic sample, 75 have been classified as foreground dK and dM contaminants. The majority (72) of these sources are in the outer region. This illustrates that the $(J-H)_0 = 0.72$ mag cut does not fully remove the foreground, confirming what we had inferred from the radial density distributions in Paper I. The colour–colour diagram in the bottom right panel of Fig. 9 shows that the majority of the dwarf sources in our spectroscopic sample have $(J-H)_0 < 0.80$ mag. If a cut was made here, 82% of the spectroscopic dwarf sample would be excluded. However, a $(J-H)_0$ cut at 0.80 mag was rejected in Paper I, as it was concluded that it would dramatically skew the derived C/M ratio; it was thought that it would reduce the number of M-type AGB sources by 63% while the number of C-type sources was reduced by only 7% (without any statistical adjustment). However, we have now confirmed that a non-negligible number of C-type stars lie blueward of the Paper I colour boundary at $(J-K)_0 = 1.20$ mag, and as a consequence approximately 30% of these sources also have colours bluer than $(J-H)_0 = 0.80$ mag. Owing to the lack of M-type giants in our spectroscopic sample, we cannot say what percentage of genuine M-type giants would be removed.

As, with one exception, all of our dwarf sources were classified photometrically as M-type giants, it may seem reasonable to conclude that the photometric M-type population is more heavily contaminated by foreground interlopers than the C-type population. However, it must be remembered that the sources in the inner region were chosen to be in the catalogue of Letarte et al. (2002). As these stars had already been classified using the CN–TiO data, they were unlikely to be foreground dwarf sources. Therefore the foreground contamination in the inner region of the spectroscopic sample does not give a true indication of the level of foreground sources among the photometric C-type sample. While the spectroscopic targets in the outer region were selected only on the basis of *JHK* photometry, the number of genuine AGB sources is expected to decline rapidly at this radius. The apparently high numbers of foreground interlopers in the outer region may therefore be a reflection of the low density of genuine sources, rather than an indicator that a redder $(J-H)_0$ cut is needed.

5.1.4. The blue limit

K_0-band magnitude and $(J-K)_0$ colour were the primary criteria by which sources in Paper I were classified. As a result our spectroscopic targets have magnitudes $K_0 \leq 17.41$ mag – the magnitude of the tip of the red giant branch (TRGB) determined in Paper I – and we cannot comment on the distribution of AGB stars fainter than this limit. However, we briefly examine the impact of the alternative colour and magnitude cuts discussed in Paper I.

In Sects. 4.1.1 and 4.2.1 we presented the colour and magnitude distributions of our spectroscopic sample. We now consider what effect the different $(J-K)_0$, K_0- and J_0-band criterion considered in Paper I would have on this sample. In Paper I a blue limit of $(J-K)_0 = 0.74$ mag was used to exclude late K-type stars and other interlopers from the AGB sample. The lack of K-type giant stars in our sample could indicate that this criterion has been successful, but is more likely to be the result of the C-type bias in our target selection (Sect. 5.1.1). Kacharov et al. (2012) find three K-type giants in their spectroscopic sample, all of which have colours $(J-K)_0 > 0.96$ mag.

5.2. Carbon stars in NGC 6822 and the Letarte et al. (2002) study

5.2.1. Estimated misclassification error

In Paper I we cross matched our photometric catalogues with the (CN–TiO) catalogue of Letarte et al. (2002) (see Sect. 2.1). We found 870 sources common to both samples and were able to classify 851 of them (717 C-type and 134 M-type sources). An estimate of the potential level of misclassification in our photometric sample was then made. It was determined that in the worst case scenario up to ~20% of the genuine C-type stars in our photometric catalogue may have been misclassified as M-type stars. However, this estimate was made by adjusting our sample to include all of the sources that were matched with counterparts in the catalogue of Letarte et al. (2002) regardless of the reliability of their photometry. If we consider only those sources that we matched with Letarte et al. (2002) and that have been flagged as stellar or probably-stellar in at least two bands (Sect. 5.1.2) then

the estimated level of misclassification for the C-type giant stars in Catalogue 1 of Paper I is reduced to 16%.

The error estimates were made based on the assumption that the spectral classifications assigned by Letarte et al. (2002) were correct in all cases. We have now shown that there is an error of ∼7% in the catalogue of Letarte et al. (2002) (Sect. 4.1.4). Moreover, classification errors are more common at bluer colours. We therefore revise our estimate of the error associated with our count of the C-type giant population in NGC 6822 down to 8%. The associated C/M and [Fe/H] values for the inner 4 kpc become 0.71 ± 0.03 and −1.32 ± 0.06 dex as a result, including the statistical foreground correction. The quoted values are for comparison with Paper I and are based on the quality control and classification criteria used in that paper.

5.2.2. Enlarged C-type giant sample

Using our spectroscopic data, we have been able to verify the accuracy of the CN–TiO method for selecting C-type stars. Now, using the catalogue of Letarte et al. (2002), we are able to significantly increase the sample of C-type stars with *JHK* photometry. We have identified 635 sources common to our Catalogue 1 (Paper I) and the catalogue of Letarte et al. (2002) and a further 97 common to Letarte et al. (2002) and Catalogue 3 (Paper I), which contains a high number of sources that we excluded from our analysis in Paper I. For ease of reference we shall refer to these photometric samples as LP1 (635 sources) and LP2 (97 sources) respectively. These common sources were identified on the basis of their astrometry, where only sources within 1.5″ (or less) of each other were considered a match. Based on the success of the CN–TiO method, we are confident that these sources have a high probability (∼98%) of being genuine C-type stars. Using our photometric data we can now examine the colour and magnitude distributions of >700 C-type stars, providing an important insight into the NIR characteristics of the wider C-type star population.

The colour and magnitude restrictions applied to the C-type sources in LP1 do not apply to the LP2 sample. Their photometric characteristics are nevertheless quite similar, indicating that neither is seriously biased photometrically. The $(J-K)_0$ colour range is 0.83−3.73 mag so does not approach the blue limit of $(J-K)_0 = 0.74$ mag imposed in Paper I. Few sources have $(J-K)_0 > 2.0$ mag, and the colour distribution peaks between 1.10−1.60 mag with more than 80% of the C-type stars having $(J-K)_0 > 1.20$ mag (top panel, Fig. 19). The C-type stars extend from $K_0 = 14.57$ to 17.28 mag, just above the TRGB.While the $(J-H)_0$ colour distribution covers the range $(J-H)_0 = 0.61$−1.97 mag, excluding two very blue outliers at −0.91 and 0.05 mag, the majority (∼90%) have $(J-H)_0 \geq 0.80$ mag.

5.3. Comparison with Kacharov et al. (2012)

5.3.1. Selection criteria

Targeting stars which $K_0 < 17.45$ mag and $(J-K)_0 > 0.74$ mag, Kacharov et al. (2012) collected spectra of ∼540 sources in the direction of NGC 6822, which had previously been classified as C- and M-type AGB stars using *JHK* photometry. Following analysis their spectroscopic sample was found to contain 151 C-type and 123 M-type giants, while the remaining spectra were those of foreground dwarf stars and a few K-type giants.

Kacharov et al. (2012) noted that the M-type giants typically had colours bluer than $(J-K)_0 = 1.20$ mag with the maximum number of sources falling between 1.00−1.10 mag, and a significant number falling between 0.90 and 1.00 mag. C-type stars were seen on either side of this colour boundary with the bluest sources having $(J-K)_0$ colours of 0.86 mag, although the majority (79%) had $(J-K)_0 > 1.20$ mag. Foreground dwarf sources in their sample were found generally to have colours between $(J-K)_0 = 0.73$−1.05 mag, with the majority having colours between $(J-K)_0 = 0.80$−0.90 mag. These findings are in good agreement with our own.

Based on their spectroscopic sample and previous work by Sibbons et al. (2011), Kacharov et al. (2012) classified sources having colours $(J-H)_0 > 0.73$ mag and $(J-K)_0 > 0.90$ mag and $K_0 < 17.45$ mag as AGB star candidates. They then proposed two different selection criteria for the classification of C- and M-type stars using cuts in $(J-K, K)_0$. The suggested criteria are shown in Fig. 18, applied to our spectroscopic sample. Kacharov et al. (2012) found that both selection criteria cleanly selected C- and M-type stars but that criteria II (bottom panel, Fig. 18) was particularly successful. Applying both criteria I and II to our spectroscopic sample we agree that the second set of criteria is better for the selection of C-type stars. However, both criteria classify >85% of the 732 C-type stars in LP1 and LP2 correctly and both criteria classify a significant number of dwarf sources as M-type giants.

5.3.2. M-type giants

The M-type giant sources of Kacharov et al. have $(J-K)_0$ colours in the range 0.81−1.31 mag, with the majority lying between 0.90−1.10 mag. The colour distribution of this sample of M-type giants relative to those of our spectroscopic C-type and dwarf sources, as well as those sources in samples LP1 and LP2, can be seen in Fig. 19. The middle panel of this figure clearly shows the expected overlap between the confirmed C- and M-type giant sources, as well as that between the M-type giant and dwarf sources noted by Kacharov et al. (2012). In combination with the top panel it can also be seen that a cut between $(J-K)_0 = 1.10$ and 1.20 mag would provide the cleanest separation between the oxygen- and carbon-rich spectral types. The M-type sources presented by Kacharov et al. (2012) have $(J-H)_0$ colours in the range = 0.63−1.07 mag, and like our spectral and photometric C-type (LP1 and LP2) samples a significant proportion (75%) have $(J-H)_0 \geq 0.8$ mag.

5.4. New JHK criteria

5.4.1. The foreground

The majority of the dwarf sources in our spectroscopic sample have $(J-K)_0 < 1.0$ mag and $(J-H)_0 < 0.80$ mag, while the majority of the C-type giants in our spectral and photometric samples and the M-type giants of Kacharov et al. (2012) have $(J-H)_0 \geq 0.80$ mag and $(J-K)_0 \geq 0.90$−1.0 mag. We therefore consider colour cuts at $(J-H)_0 = 0.80$ mag and $(J-K)_0 = 1.0$ mag, in an effort to reduce the number of foreground stars in our sample.

Applying first the $(J-H)_0$ cut, we find that 80% of the 75 dwarf sources in our spectroscopic sample are removed and a further 13% (10 sources) are removed when the $(J-K)_0$ cut is applied. However, we also find that 31 (25%) M-type sources and 26 (32%) C-type sources are removed by this $(J-H)_0$ cut and these numbers increase to 49 and 27 respectively when the $(J-K)_0$ cut is applied. The loss of so many genuine AGB sources is unacceptable. In order to establish an optimal set of cuts, we

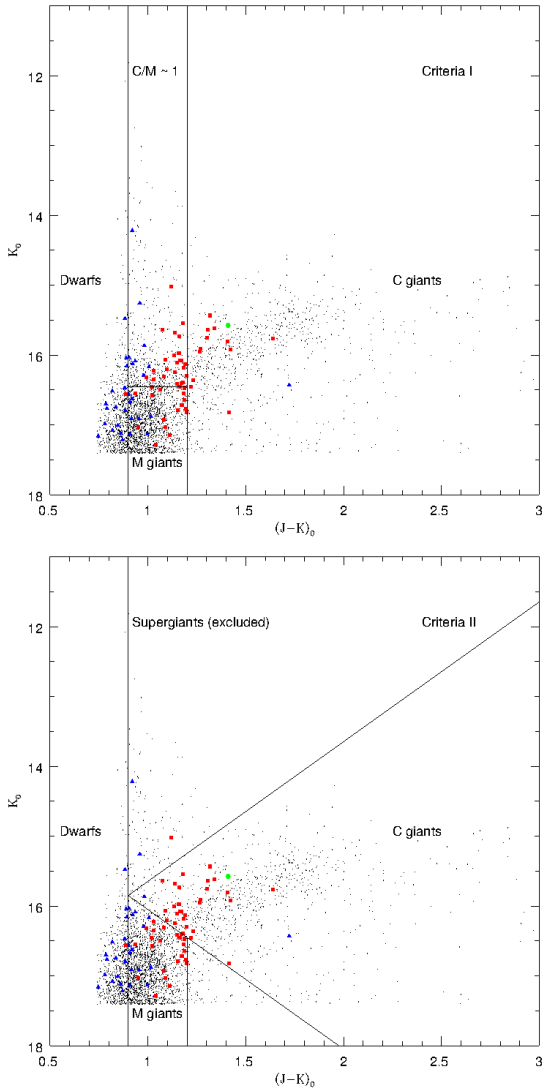

Fig. 18. *Top*: CMD of our spectroscopic sources overlayed on the sources from Catalogue 1 of Paper I. Red squares are C-type stars, blue triangles are M- and K-type dwarf stars and the green hexagon is the only M-type giant in our sample. The solid lines represent criteria I proposed by Kacharov et al. (2012). *Bottom*: same CMD as above but the solid lines now represent criteria II proposed by Kacharov et al. (2012). Regions in both CMDs have been labelled in accordance with the CMDs of Kacharov et al. (2012).

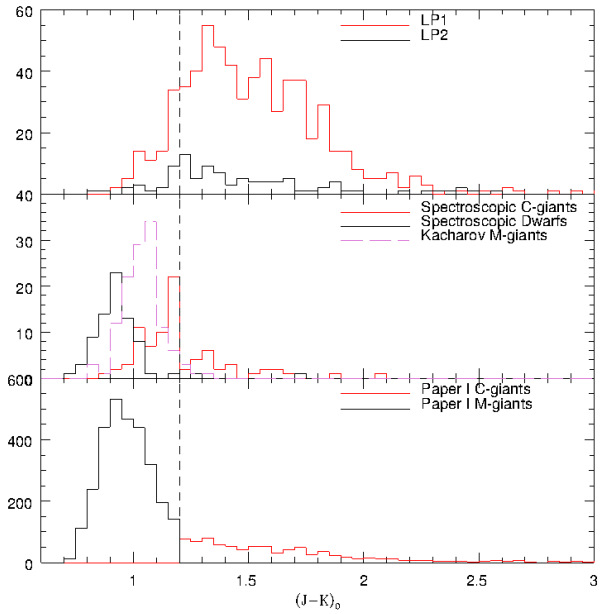

Fig. 19. $(J-K)_0$ colour histograms in 0.05 mag bins. *Top*: the distributions of the LP1 (red) and LP2 (black) samples. *Middle*: colour histograms for the spectroscopic sample presented here. The K- and M-type dwarf sources (black) and the C-type sources (red). A colour histogram (purple) for the spectroscopically confirmed M-type giants of Kacharov et al. (2012) is also shown. *Bottom*: as above for the sources classified as M-type (black) and the sources classified as C-type (red) in Catalogue 1 of Paper I. The dashed vertical line at $(J-K)_0 = 1.20$ mag marks the position of the colour boundary used in Paper I.

reviewed the impact of cuts in $(J-H)_0$ between 0.72–0.80 mag at 0.02 mag intervals, in conjunction with cuts in $(J-K)_0$ between 0.9 and 1.0 mag, also at 0.02 mag intervals. The impact of one set of these cuts on the retention of dwarf and giant sources is shown in Table 8. In total over thirty $(J-H)_0$ and $(J-K)_0$ colour cut combinations were considered and it was established that the best results for the selection of giant sources were obtained using cuts at $(J-H)_0 \geq 0.76$ mag and $(J-K)_0 \geq 0.93$ mag in partnership with the magnitude cut at $K_0 = 17.41$ mag.

The overlap between the giant and dwarf sources in the $(J-K, K)_0$ CMD and the $(H-K, J-H)_0$ colour–colour diagram (Fig. 20) demonstrates that there is no single colour cut in either $(J-H)_0$ or $(J-K)_0$ that will completely separate the two populations. From Table 8 we see that ~25% of the dwarf sources in our (biased) spectral data set are retained using the proposed colour cuts. While this may appear to be a significant proportion, it must be remembered that this fraction is artificially exaggerated by our limited sample and by the bias in our source selection; in reality these sources represent a very small fraction of the whole dwarf population, the majority of which was removed by the $(J-H)_0 \geq 0.72$ mag cut in Paper I.

The effectiveness of these colour criteria can also be estimated by establishing what percentage of the sources retained as NGC 6822 giants that are actually foreground dwarf stars. Using our spectroscopic sample and that of Kacharov et al. (2012) for the M-type giants, this fraction is estimated to be ~9%.

5.4.2. C- and M-type giant selection

The C-type giants in the spectroscopic catalogue of Kacharov et al. (2012) and the photometric LP1 and LP2 samples show that the majority of C-type stars lie redward of $(J-K)_0 = 1.20$ mag. Nevertheless we re-examine the $(J-K)_0$ colour distributions of our spectroscopically confirmed C-type stars and the M-type giants of Kacharov et al. (2012), as well as our photometric C-type star sample (LP1 and LP2) to try to establish a better colour boundary between the two spectral types.

In the middle panel of Fig. 19 we see that the number of M-type giant sources declines sharply at $(J-K)_0 \geq 1.10$ mag, while the number of C-type sources increases suddenly at $(J-K)_0 \geq 1.15$ mag. Placing the colour boundary at $(J-K)_0 = 1.15$ mag therefore seems appropriate from an empirical perspective.

In order to better establish the position of the colour boundary we have examined the impact of placing the boundary at different positions between $(J-K)_0 = 1.10$ and 1.20 mag at 0.01 mag intervals. Specifically we have looked at the number of sources misclassified (e.g. a C-type star as an M-type star or vice versa) in each of the following data sets; 1) the spectroscopically confirmed C-type stars that have $(J-K)_0 < 1.20$ mag (i.e.

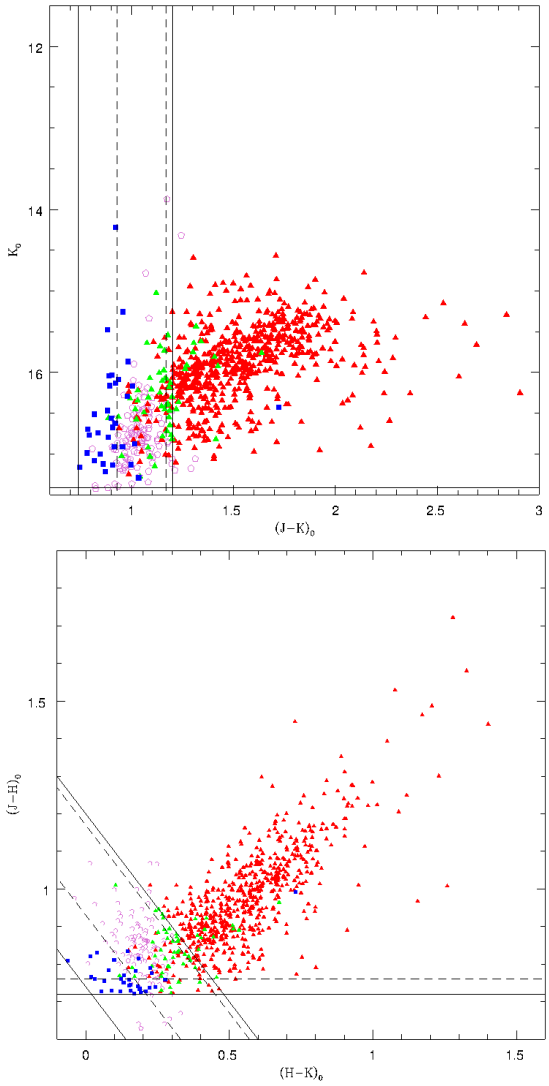

Fig. 20. *Top*: CMD of our spectroscopically confirmed dwarf (blue squares) and C-type giant (green triangles) sources, the M-type giant (purple circles) sources of Kacharov et al. (2012) and the photometric C-type giants (red triangles) of the LP1 sample. The solid horizontal and vertical lines mark the TRGB and $(J-K)_0$ criterion at 0.74 and 1.20 mag used in Paper I. The two dashed lines mark the new $(J-K)_0$ cuts at 0.93 mag and 1.17 mag (see Sect. 5.4.2). *Bottom*: colour–colour diagram of the same sources. The solid horizontal and diagonal lines mark the $(J-H)_0 = 0.72$ mag and $(J-K)_0 = 0.74$ and =1.20 mag criteria used in Paper I. The horizontal dashed line marks the new cut at $(J-H)_0 = 0.76$ and the two diagonal dashed lines mark the new cuts at $(J-K)_0 = 0.93$ mag and 1.17 mag.

those C-type sources that were misclassified in Paper I); 2) the C-type sources in samples LP1 and LP2; and 3) the spectroscopically confirmed set of M-type giants published by Kacharov et al. (2012). The percentages of each of these populations misclassified at each colour boundary have been calculated and are presented in Table 9. We have examined both the spectroscopic and photometric C-type stars samples, as while the spectroscopic sample is highly reliable its colour distribution is biased for the reasons we have discussed and the sample is small in size. On the other hand the photometric sample is larger and unbiased but is less reliable.

Each proposed colour boundary shown in Table 9 has been applied, in conjunction with our other newly proposed criteria (Sects. 5.1.2 and 5.4.1), to the original photometric catalogue

Table 8. Percentage of spectroscopically confirmed sources retained when various blue limit $(J-K)_0$ cuts are applied in addition to a colour cut at $(J-H)_0 = 0.76$ mag.

$(J-K)_0$	C-type giants	M-type giants	Dwarf sources
0.90	87%	85%	30%
0.92	87%	84%	25%
0.94	84%	81%	23%
0.96	83%	80%	19%
0.98	83%	72%	17%
1.00	82%	67%	13%

Notes. These percentages relate to the spectroscopically confirmed dwarf and C-type giant samples (Tables 10 and 11) and M-type giant sample of Kacharov et al. (2012).

Table 9. Percentage classification error in the photometric and spectroscopic samples.

$(J-K)_0$ mag	Spec. C-type giants misc.	Phot. C-type giants misc.	M-type giants misc.
1.10	33% (44%)	3% (5%)	21% (18%)
1.11	35% (46%)	4% (6%)	18% (15%)
1.12	37% (47%)	4% (6%)	18% (13%)
1.13	43% (53%)	4% (7%)	15% (11%)
1.14	50% (58%)	5% (7%)	13% (9%)
1.15	50% (60%)	5% (8%)	10% (9%)
1.16	61% (68%)	6% (8%)	10% (9%)
1.17	67% (74%)	7% (9%)	10% (7%)
1.18	78% (82%)	8% (11%)	8% (7%)
1.19	89% (91%)	9% (12%)	8% (4%)
1.20	100% (100%)	11% (14%)	5% (4%)

Notes. For each of the three samples discussed in text (Sect. 5.4.2) we have listed the percentage of sources misclassified at each of the colour boundaries listed in the first column. These percentages have been calculated after the application of the new $(J-H)_0$ and blue limit $(J-K)_0$ cuts outlined in Sect. 5.4.1 and the TRGB magnitude cut at $K_0 \leq 17.41$ mag. In brackets we show the percentage of misclassifications if only the $(J-K)_0$ cut in the first column and no other criteria are applied.

used in Paper I to establish the distribution of C/M ratios resulting from the different boundaries. Calculating an average C/M ratio (∼0.94) from this distribution we have then been able to interpret the impact of varying the colour boundary and the resulting rates of misclassification on the C/M ratio and have concluded that a colour boundary between $(J-K)_0 = 1.16$ and 1.18 mag would be most suitable.

Based on a mean C/M ratio of ∼0.94 and the $(J-K)_0$ colour distributions shown in Fig. 19, we have determined that the colour boundary between the C- and M-type AGB stars is best placed at $(J-K)_0 \sim 1.17$ mag. While we cannot avoid all cross-contamination between the C- and M-type populations, by placing the boundary here we do hope to ensure, as far as possible, that on average approximately equal numbers of each type of star are misclassified and therefore minimise the error in the calculated C/M ratio.

5.4.3. Catalogue 1 revisited

Our new photometric selection criteria have been applied to the original *JHK* photometry used in Paper I. Using the two band quality flag criteria, while still requiring the sources to have

magnitude measurements in all three photometric bands, we reduced the original catalogue of ∼375 000 sources by ∼50%. From this reduced catalogue we select 2905 candidate AGB stars across the full observed area (3 deg^2) using colour cuts at $(J-H)_0 \geq 0.76$ mag and $(J-K)_0 \geq 0.93$ mag and a magnitude cut at the TRGB magnitude established in Paper I ($K_0 \leq 17.41$ mag). We then separate this sample into 1590 M-type stars with $(J-K)_0 < 1.17$ mag and 1315 C-type stars with $(J-K)_0 \geq 1.17$ mag.

As in Paper I, we apply the 4 kpc radial limit, reducing the number of C- and M-type stars to 1049 and 1149, respectively. Without any statistical correction for the remaining foreground contaminants we then derive a C/M ratio of 0.91 ± 0.04 and an iron abundance of −1.37 ± 0.06 dex.

As some foreground contaminants are still expected to be present in this sample, a statistical adjustment is made to the number of C- and M-type as was done in Paper I. It was found that there were ∼3 apparent foreground M-type stars per kpc^2 and ∼2 foreground apparent C-type stars per kpc^2. With the implementation of these statistical adjustments, the C/M ratio inside the 4 kpc limit increases to 0.95 ± 0.04 and the derived [Fe/H] value becomes −1.38 ± 0.06 dex, 0.09 dex lower than the value we derived in Paper I. This value has been derived using the C/M vs. [Fe/H] relation of Cioni (2009), but for comparison we note that when using the relations of Cioni & Habing (2003, 2005) and Battinelli & Demers (2005) the calculated values for the iron abundance lie between −1.0 and −1.31 dex in the central 4 kpc of the galaxy.

The values we derive for the C/M ratio and [Fe/H] are appreciably different from those presented in Paper I. The iron abundance we derive here is more consistent with previous estimates of the metallicity of the RGB population which ranges between −1.0 (Tolstoy et al. 2001; Davidge 2003a) and −1.50 dex (Gallart et al. 1996). Above all the values we derive here emphasise the sensitivity of the C/M ratio to the selection criteria when using the *JHK* photometry and the difficulties of selecting an uncontaminated sample of sources that is representative of the population.

6. Conclusions

Spectra of 162 sources previously classified as AGB candidates, using either *JHK* photometry or the CN–TiO method, have been presented. Based on this sample and others in the literature we have reviewed the effectiveness of the *JHK* selection criteria derived in Paper I of this series and tested the validity of the 4 kpc radial limit imposed in the same paper. From there we have derived new selection criteria and calculated new values for the global C/M ratio and iron abundance in NGC 6822. In addition we have also provided the first estimate of the level of error in the catalogue of C-type stars presented by Letarte et al. (2002).

Our main conclusions are as follows:

1. Of the 160 sources in our spectroscopic sample previously classified as AGB giants of spectral type C or M, 75 (∼47%) were identified as foreground interlopers. We therefore re-evaluated the colour criterion used to exclude contaminants from the initial photometric sample. Based on the $(J-H)_0$ and $(J-K)_0$ colour distributions of the sources in our own spectroscopic sample and that of Kacharov et al. (2012), as well as the colour distributions of a large, reliable photometric sample of C-type stars, we now make cuts at $(J-H)_0 \geq 0.76$ mag ($(J-H)_{2MASS} \geq 0.79$ mag) and $(J-K)_0 \geq 0.93$ mag ($(J-K_s)_{2MASS} \geq 0.98$ mag). These cuts are made in conjunction with a magnitude cut at the TRGB ($K_0 = 17.41$ mag), the position of which was established in Paper I, in order to isolate the AGB population.
2. The position of the $(J-K)_0$ colour boundary used to classify AGB sources as either C- or M-type was also re-evaluated as our spectroscopic sample has revealed a tail of C-type giants extending up to 0.30 mag blueward of the $(J-K)_0 = 1.20$ mag colour boundary imposed in Paper I. Based on the $(J-K)_0$ colour distributions of the different populations examined here and our analysis of the misclassifications rates in these populations when using different colour boundaries, a new colour boundary of $(J-K)_0 = 1.17$ mag ($(J-K_s)_{2MASS} = 1.24$ mag) has been established.
3. We have also been able to test the validity of the 4 kpc radial limit imposed in Paper I. Measurements of the radial velocity have show a difference of −39.3 ± 9.8 km s^{-1} between the mean heliocentric velocity of those sources within 3 kpc of the galactic centre and those sources in the outer region. Furthermore, from the spectra of individual stars, only three of the 75 sources at a distance of ≥5 kpc from the centre of the galaxy were identified as giants. The lack of giant stars in the outer region echos the findings of Kacharov et al. (2012), and supports our conclusion in Paper I that the decline in the stellar density between 4–5 kpc is not the beginning of an extended halo of RGB stars. We therefore conclude that although a radial limit of 4 kpc may be conservative it is appropriate.
4. The revised *JHK* selection criteria have been applied to the same photometric data used in Paper I and a new value of 0.95 ± 0.04 has been calculated for the C/M ratio within 4 kpc of the centre of NGC 6822. Using the C/M vs. [Fe/H] relation of Cioni (2009) a new estimate of the global iron abundance has also been made; [Fe/H] = −1.38 ± 0.06 dex. This is 0.09 dex more metal poor than the estimate we presented in Paper I but is still, within errors, in agreement with previous metallicity estimates of the old- and intermediate-age population of NGC 6822.
5. By including in our spectroscopic sample 85 sources previously classified as C-type giants by Letarte et al. (2002) using the CN–TiO method, we have been able to compare the CN–TiO and *JHK* methods. The CN–TiO method was found to have the higher success rate, correctly classifying 93% of candidates. However, while the CN–TiO method has been confirmed to be highly reliable for the classification of C-type AGB stars it is not infallible and we are able to present a first estimate of the error associated with that method (∼7%).

The C/M ratio in conjunction with *JHK* photometry could be very useful for examining the mean metallicity of an AGB population. However, further improvements are required if this method is to be exploited to its full potential by the astronomical community. First, it is dependent on the reliable classification of sources as either C- or M-type stars. We have shown that for the selection of C-type stars at least, that the CN–TiO method is more reliable than *JHK* photometry. Therefore, if we wish to make the best use of the many forthcoming NIR optimised instruments we must continue to refine the criteria for the selection of AGB sources in the NIR. Second, we have shown that a relatively large change in the C/M ratio (∼50%) results in only a minor change (∼0.1 dex) in the calculated iron abundance for the galaxy using the C/M vs. [Fe/H] relation of Cioni (2009). The situation is not improved when other relationships available

in the literature are applied. Clearly, a tighter relation between these two variables is needed if the C/M ratio is to be used for anything other than to gain a very broad overview of galactic metallicity.

Acknowledgements. We would like to thank the following people for their assistance during this work; Scott Croom (SIfA, University of Sydney) who was the telescope operator when our observations were taken and Sarah Brough (AAO) for her assistance in reducing the observations. Patricia Whitelock (SAAO/UCT) for providing valuable insight into the nature of symbiotic stars and Nikolay Kacharov of the University of Heidelberg, and collaborators, for providing us with their results prior to publication. Finally, we would like to thank the referee for his/her detailed reading of this paper and the useful comments they provided.

References

Allen, D. A. 1984, Proc. Astron. Soc. Aust., 5, 369
Battinelli, P., & Demers, S. 2005, A&A, 434, 657
Battinelli, P., & Demers, S. 2011, A&A, 525, A69
Battinelli, P., Demers, S., & Kunkel, W. E. 2006, A&A, 451, 99
Belczyński, K., Mikołajewska, J., Munari, U., Ivison, R. J., & Friedjung, M. 2000, A&AS, 146, 407
Bessell, M. S., & Brett, J. M. 1988, PASP, 100, 1134
Blanco, B. M., Blanco, V. M., & McCarthy, M. F. 1978, Nature, 271, 638
Brewer, J. P., Richer, H. B., & Crabtree, D. R. 1995, AJ, 109, 2480
Brewer, J. P., Richer, H. B., & Crabtree, D. R. 1996, AJ, 112, 491
Brewer, J. P., Richer, H. B., & Crabtree, D. R. 2000, in IAU Symp., 177, The Carbon Star Phenomenon, ed. R. F. Wing, 59
Cioni, M. 2009, A&A, 506, 1137
Cioni, M., & Habing, H. J. 2003, A&A, 402, 133
Cioni, M., & Habing, H. J. 2005, A&A, 429, 837
Clementini, G., Held, E. V., Baldacci, L., & Rizzi, L. 2003, ApJ, 588, 85
Cohen, M. 1980, ApJ, 238, L81
Cook, K. H., Aaronson, M., & Norris, J. 1986, ApJ, 305, 634
Corradi, R. L. M., Brandi, E., Ferrer, O. E., & Schwarz, H. E. 1999, A&A, 343, 841
Corradi, R. L. M., Rodríguez-Flores, E. R., Mampaso, A., et al. 2008, A&A, 480, 409
Corradi, R. L. M., Valentini, M., Munari, U., et al. 2010, A&A, 509, A41
Corradi, R. L. M., Sabin, L., Munari, U., et al. 2011, A&A, 529, A56
Crowe, R. A. 1983, J. Am. Assoc. Var. Star Obs., 12, 58
Danks, A. C., & Dennefeld, M. 1994, PASP, 106, 382
Davidge, T. J. 2003a, ApJ, 597, 289
Davidge, T. J. 2003b, PASP, 115, 635
Demers, S., Battinelli, P., & Artigau, E. 2006, A&A, 456, 905
Gallart, C., Aparicio, A., & Vilchez, J. M. 1996, AJ, 112, 1928
García-Hernández, D. A., Karakas, A. I., & Lugaro, M. 2013, Mem. Soc. Astron. It., 84, 216
Garrison, R. F. 1997, J. Am. Assoc. Var. Star Obs., 25, 70
Gonçalves, D. R., Magrini, L., Munari, U., Corradi, R. L. M., & Costa, R. D. D. 2008, MNRAS, 391, L84
Groenewegen, M. A. T. 2006, in Planetary Nebulae Beyond the Milky Way, eds. L. Stanghellini, J. R. Walsh, & N. G. Douglas (Berlin: Springer), 108
Groenewegen, M. A. T., Lançon, A., & Marescaux, M. 2009, A&A, 504, 1031
Gurzadyan, G. A. 1977, Ap&SS, 52, 51
Hawley, S. L., Gizis, J. E., & Reid, I. N. 1996, AJ, 112, 2799
Hodgkin, S. T., Irwin, M. J., Hewett, P. C., & 1 Warren, S. J. 2009, MNRAS, 394, 675
Hwang, N., Lee, M. G., Lee, J. C., et al. 2005, in Near-fields cosmology with dwarf elliptical galaxies, eds. H. Jerjen, & B. Binggeli, IAU Colloq. 198, 257
Iben, Jr., I., & Renzini, A. 1983, ARA&A, 21, 271
Irwin, M. J., Lewis, J., Hodgkin, S., et al. 2004, in SPIE Conf. Ser. 5493, eds. P. J. Quinn, & A. Bridger, 411
Izzard, R. G., & Poelarends, A. J. T. 2006, Mem. Soc. Astron. It., 77, 840
Jacoby, G. H., Hunter, D. A., & Christian, C. A. 1984, ApJS, 56, 257
Joergens, V., Kopytova, T., & Pohl, A. 2012, A&A, 548, A124
Kacharov, N., Rejkuba, M., & Cioni, M.-R. L. 2012, A&A, 537, A108
Kang, A., Sohn, Y., Kim, H., et al. 2006, A&A, 454, 717
Karakas, A. I., García-Hernández, D. A., & Lugaro, M. 2012, ApJ, 751, 8
Kirkpatrick, J. D., Henry, T. J., & McCarthy, Jr., D. W. 1991, ApJS, 77, 417
Kniazev, A. Y., Väisänen, P., Whitelock, P. A., et al. 2009, MNRAS, 395, 1121
Komiyama, Y., Okamura, S., Yagi, M., et al. 2003, ApJ, 590, 17
Lee, M. G., Freedman, W. L., & Madore, B. F. 1993, ApJ, 417, 553
Leedjärv, L., Burmeister, M., Mikołajewski, M., et al. 2004, A&A, 415, 273
Letarte, B., Demers, S., Battinelli, P., & Kunkel, W. E. 2002, AJ, 123, 832
Looper, D. L., Bochanski, J. J., Burgasser, A. J., et al. 2010, AJ, 140, 1486
Massey, P., Armandroff, T. E., Pyke, R., Patel, K., & Wilson, C. D. 1995, AJ, 110, 2715
Mateo, M. L. 1998, ARA&A, 36, 435
Osterbrock, D. E. 1988, PASP, 100, 412
Palmer, L. G., & Wing, R. F. 1982, AJ, 87, 1739
Peimbert, A., Peimbert, M., & Ruiz, M. T. 2005, ApJ, 634, 1056
Phillips, J. P. 2007, MNRAS, 376, 1120
Renzini, A., & Buzzoni, A. 1986, in Spectral Evolution of Galaxies, eds. C. Chiosi & A. Renzini, Astrophys. Space Sci. Lib., 122, 195
Richer, H. B., Olander, N., & Westerlund, B. E. 1979, ApJ, 230, 724
Richer, H. B., Crabtree, D. R., & Pritchet, C. J. 1984, ApJ, 287, 138
Roeser, S., Demleitner, M., & Schilbach, E. 2010, AJ, 139, 2440
Saunders, W., Bridges, T., Gillingham, P., et al. 2004, in SPIE Conf. Ser. 5492, eds. A. F. M. Moorwood, & M. Iye, 389
Scalo, J. M., & Miller, G. E. 1981, ApJ, 248, L65
Schlegel, D. J., Finkbeiner, D. P., & Davis, M. 1998, ApJ, 500, 525
Schmid, H. M. 1989, A&A, 211, L31
Shaw, R. A., & Dufour, R. J. 1994, in Astronomical Data Analysis Software and Systems III, eds. D. R. Crabtree, R. J. Hanisch, & J. Barnes, ASP Conf. Ser., 61, 327
Sibbons, L. F., Cioni, M.-R. L., Irwin, M., & Rejkuba, M. 2011, in Why Galaxies Care about AGB Stars II: Shining Examples and Common Inhabitants, Proc. Conf. Viena, eds. F. Kerschbaum, T. Lebzelter, & R. F. Wing (San Francisco: ASP), 445, 409
Sibbons, L. F., Ryan, S. G., Cioni, M.-R. L., Irwin, M., & Napiwotzki, R. 2012, A&A, 540, A135
Smith, G. A., Saunders, W., Bridges, T., et al. 2004, in SPIE Conf. Ser. 5492, eds. A. F. M. Moorwood, & M. Iye, 410
Sohn, Y., Kang, A., Rhee, J., et al. 2006, A&A, 445, 69
Stancliffe, R. J. 2010, MNRAS, 403, 505
Tolstoy, E., Irwin, M. J., Cole, A. A., et al. 2001, MNRAS, 327, 918
Turnshek, D. E., Turnshek, D. A., Craine, E. R., & Boeshaar, P. C. 1985, An atlas of digital spectra of cool stars (Types G, K, M, S and C) (Western Research Company)
Venn, K. A., Lennon, D. J., Kaufer, A., et al. 2001, ApJ, 547, 765
Whitelock, P. A., & Munari, U. 1992, A&A, 255, 171
Whitelock, P. A., Menzies, J. W., Feast, M. W., Nsengiyumva, F., & Matsunaga, N. 2013, MNRAS, 428, 2216

Pages 26 to 33 are available in the electronic edition of the journal at http://www.aanda.org

Table 1. Atomic and molecular features used to classify C, M- and S-type stars.

λ (Å)	Feature	Comment
4861	Hβ F-line	Fraunhofer F-line. Seen in emission in some of our stars.
4959	[O III]	Forbidden emission line of doubly ionised oxygen, ~1/3 strength of the 5007 Å line. Seen in some of our stars.
5007	[O III]	Forbidden emission line of doubly ionised oxygen. Seen in some of our stars.
5165	C_2	Degrades blueward from bandhead.
5167	Mg I	Visible in all G, K, and M-type stars until M4 III or M6.5 V; greatly enhanced in dwarfs.
5173	Mg I	See comments for Mg I 5167 Å.
5184	Mg I	See comments for Mg I 5167 Å.
5211	MgH	Broad absorption feature in M-type dwarfs; degrades toward the violet.
5298	ZrO	Several ZrO bands beginning at 5298 Å. Visible in mid S-type stars.
5577	[O I]	Telluric oxygen emission line.
5636	C_2	Degrading blueward.
5730	CN	
5810	TiO	Visible at M2 to M3.
5862	TiO	Visible at M0 to M1.
5890	Na I D-line	Visible in all G-, K- and early M-type stars. Greatly enhanced in dwarfs; overwhelmed in M-type giants by M2.
5896	Na I D-line	As above.
6005	C_2	Molecular carbon feature degrading blueward.
6059	C_2	Molecular carbon feature degrading blueward.
6132	ZrO	Several ZrO bands beginning at 6132 Å. Increasing in strength with later spectral type.
6159	TiO	Bandhead degrades redward.
6162	Ca I	Enhanced in M-type dwarfs.
6206	CN	
6300	[O I]	Telluric oxygen line.
6332	CN	
6363	[O I]	Telluric oxygen emission line.
6385	CaH	Band used as an M-type dwarf indicator.
6478	CN	
6532	VO	Seen in S-type stars.
6548	[N II]	Forbidden emission line of singly ionised nitrogen, ~1/3 strength of the 6583 Å line. Seen in some of our stars.
6563	Hα C-line	Fraunhofer C-line. Seen in emission or absorption in some of our stars.
6569	TiO	Several TiO bands beginning at 6569 Å that are marginally visible in early M-types.
6583	[N II]	Forbidden emission line of singly ionised nitrogen. Seen in some of our stars.
6631	CN	
6716	[S II]	Forbidden emission line of singly ionised sulphur. Seen in some of our stars.
6731	[S II]	As above.
6867	O_2 *B*-band	Fraunhofer B-line. A telluric absorption feature.
6908	CaH	Discussed with CaH (6946 Å) below.
6925	CN	
6933	ZrO	Seen in S-type stars. Clearly visible by mid-S.
6946	CaH	Strongest in early M-type dwarfs. Bands of CaH serve to widen and deepen the TiO bands in this region. Blended with the O_2 *B*-band.
6988	ZrO	Seen in S-type stars. Clearly visible by mid-S.
7054	TiO	Clearly visible at K5; bandhead degrading redward.
7088	CN	
7186	H_2O	Telluric band. Degrading redward.
7198	TiO	Distinct from M1.
7219	TiO	Distinct from M1.
7259	CN	
7269	TiO	Distinct from M1. Combined with TiO bands at 7198 and 7219 Å creates a distinctive triple dip feature.
7334	VO	Several bands of VO beginning at 7334 Å and increasing in strength from late M-type stars.
7437	CN	
7590	TiO	Blended into the O_2 A-band.
7594	O_2 A-band	Fraunhofer A-line. A telluric absorption feature.
7628	TiO	Several TiO bands follow on from 7666 Å, creating a wide depression in the region immediately following the telluric. O_2 feature. Seen in M-type stars of all luminosities. First seen around M2 becoming very pronounced by mid-M.
7861	TiO	
7876	CN	Several CN bands follow on from 7876 Å. Obvious in supergiants, weaker in giants; not seen in dwarfs.
8026	CN	Several CN bands follow on from 8026 Å. Obvious in supergiants, weaker in giants; not seen in dwarfs.
8183	Na I	Strong in dwarf stars.
8195	Na I	As above.
8227	H_2O	Weak telluric feature. Degraded to the red.
8498	Ca II	Strongest in late K-type through mid M-type stars; strongest in giants and super giants; weaker in dwarfs.
8542	Ca II	As above.
8662	Ca II	As above.

Notes. The wavelengths of some of the major telluric features seen in our spectra are also listed. The most important of these features have been marked on the spectra. Comments are included, where relevant, from the work of Turnshek et al. (1985), Kirkpatrick et al. (1991) and our own observations. Also included are the wavelengths of some important emission lines seen in some of our spectra.

Table 10. 74 candidate AGB sources in the inner region (≤3 kpc) for which spectra with $S/N \geq 10$ were obtained.

ID	RA (2000.0) (deg)	Dec (2000.0) (deg)	J (mag)	H (mag)	K (mag)	Phot. type	Dist. (kpc)	Spec. type	Kmatch	Dmatch	Letarte ID	$R-I$ (mag)	CN–TiO (mag)	S/N
157078	296.117004	–14.632751	16.46	15.59	15.26	M	1.77	C:	C5.5	C	87	1.177	0.371	21
165127	296.233887	–14.671288	17.14	16.26	16.01	M	1.13	C	C3.2	C	459	1.102	0.356	12
167638	295.968842	–14.682981	16.82	16.02	15.68	M*	2.45	C	C5.5	C	3	1.214	0.469	12
167938	296.259827	–14.684196	17.31	16.47	16.21	M*	1.03	C	C5.5	C	586	1.14	0.318	14
168284	296.411377	–14.685686	17.47	16.58	16.11	C*	1.75	C:	C3.2	C	867	1.174	0.395	11
168690	296.156006	–14.687428	17.31	16.25	15.68	C*	1.20	Ce:	M1III	K4III	137	1.506	0.426	10
168826[4]	296.179413	–14.688039	17.24	16.35	16.08	M	1.10	C	C3.2	S	206	1.142	0.366	10
169202	296.248596	–14.689795	17.26	16.43	16.11	M	0.97	C	C3.2	S	531	1.295	0.364	13
170279	295.969452	–14.694445	17.32	16.40	16.13	M	2.40	C	C3.2	S	4	1.147	0.424	14
170941	296.286774	–14.697333	17.18	16.40	16.17	M*	0.99	dK	dK7	K4III	704	1.11	0.334	24
173114	296.33078	–14.707144	15.97	15.27	14.94	M*	1.13	dM:	dM0	M0V	799	1.276	0.418	28
176863	296.350922	–14.720666	17.05	16.13	15.75	C*	1.17	C	C6.5	S	827	1.518	0.385	14
180514	296.375854	–14.73088	16.15	15.33	15.03	M	1.30	C	C3.2	C	847	1.175	0.41	22
184448	296.436554	–14.743853	17.45	16.68	16.56	M*	1.72	C	C5.5	C	877	1.137	0.332	11
186430	296.234741	–14.750431	17.23	16.46	16.24	M	0.45	Uncl	dK7	K0III	464	1.132	0.329	34
188246[4]	296.485382	–14.756809	16.74	15.93	15.63	M	2.09	C:	C3.2	C	893	1.106	0.37	20
188974[2]	296.131714	–14.759347	17.37	16.47	16.18	M	0.95	Ce	C	C	100	1.159	0.352	10
193714	296.112915	–14.776258	17.35	16.46	15.92	C*	1.06	C	C5.5	C	84	1.394	0.537	14
197170	296.152313	–14.788395	17.14	16.30	15.98	M	0.72	Ce	C3.2	C	128	1.194	0.372	16
197464	296.283356	–14.789384	17.47	16.75	16.45	M	0.40	C	C5.5	K0III	693	1.3	0.43	12
197590	296.319458	–14.789786	16.99	16.07	15.58	C*	0.69	M:	M1III	M0III	788	1.48	0.609	19
199974	296.374786	–14.798067	17.73	16.79	16.55	M	1.14	C	C3.2	C	846	1.118	0.411	13
200182	296.170349	–14.798781	17.40	16.44	15.76	C*	0.56	Ce	C5.5	C	178	1.327	0.491	17
201043	296.073059	–14.801702	17.62	16.74	16.46	M	1.36	C	C3.2	C	40	1.109	0.45	10
201131	296.160095	–14.802064	17.38	16.61	16.35	M	0.64	C	C3.2	K3III	149	1.173	0.314	18
203106	296.338257	–14.808908	17.41	16.50	16.05	C*	0.83	C:	C5.5	C	810	1.215	0.359	10
206129[1]	296.238953	–14.8196	17.84	17.06	16.83	M	0.14	dKe:	dK7	K0III	486	1.252	0.454	21
208620	296.100708	–14.828527	16.72	15.96	15.64	M	1.15	C	C3.2	C	66	1.143	0.403	18
209650[2]	296.129822	–14.832311	17.56	16.74	16.49	M	0.92	C	C3.2	C	99	1.169	0.427	12
209652[2]	296.084503	–14.832314	17.50	16.60	16.15	C*	1.29	C:	C5.5	S	50	1.39	0.472	11
210316	296.434357	–14.834667	17.48	16.72	16.32	M	1.65	C:	C5.5	C	875	1.109	0.421	14
211898	296.30838	–14.840508	17.25	16.46	16.08	M	0.67	C	C3.2	C	764	1.104	0.422	17
215861	296.173828	–14.855554	17.84	16.97	16.65	M	0.69	Ce	C	C	189	1.173	0.344	11
216688	296.080383	–14.858717	16.31	15.70	15.29	M*	1.38	C:	K7III	M0III	46	1.247	0.518	28

Notes. In Col. 1 those sources with a superscript reference number are in common with the catalogues of [(1)] Kang et al. (2006), [(2)] Demers et al. (2006), [(3)] Whitelock et al. (2013) and [(4)] Kacharov et al. (2012, see Table 13) . In Col. 7 sources marked with a * were rejected from the photometric sample in Paper I as they did not meet their strict quality control criterion but nevertheless could be classified by them. In Col. 9, source classifications preceded by a "d" denote dwarf stars, "e" indicates the presence of Hα in emission – many also show [S II] and [N II] (see Sect. 4.1.2) – and a colon ":" indicates a tentative classification. The horizontal line separates those C-type sources misclassified as dK or dK7 by the matching program from the rest of the sample. A further 11 sources which showed high energy emission lines are listed in Table 4.

Table 10. continued.

ID	RA (2000.0) (deg)	Dec (2000.0) (deg)	J (mag)	H (mag)	K (mag)	Phot. type	Dist. (kpc)	Spec. type	Kmatch	Dmatch	Letarte ID	$R-I$ (mag)	CN–TiO (mag)	S/N
219351	296.28244	–14.868937	17.48	16.72	16.55	M	0.67	Ce	C3.2	C	690	1.168	0.43	13
220153	296.236908	–14.87212	18.02	17.07	16.82	M	0.59	Ce	C3.2	C	477	1.148	0.434	12
222468	296.096558	–14.8814	17.98	17.19	17.03	M	1.34	C	C5.5	C	63	1.201	0.428	12
223056	296.261414	–14.883708	17.94	17.07	16.79	M	0.72	Ce	C3.2	C	598	1.137	0.424	12
224407	296.431213	–14.889406	17.33	16.48	16.18	M	1.76	C:	C5.5	C	873	1.243	0.486	10
225648[4]	296.163086	–14.894488	16.75	15.88	15.44	C*	0.99	C	C5.5	C	158	1.373	0.559	22
226603[4]	296.118591	–14.89873	16.89	16.03	15.73	M	1.28	C	C5.5	C	88	1.203	0.383	14
228306[4]	296.251007	–14.9064	17.96	17.09	16.77	M	0.89	Ce	C	C	542	1.204	0.484	16
229643	296.35376	–14.912353	17.22	16.35	15.96	C*	1.34	C	C3.2	C	830	1.194	0.405	11
231793	296.223907	–14.922441	17.22	16.33	15.81	C*	1.03	C	C5.5	C	396	1.261	0.446	17
233186	296.157745	–14.929084	0.00	16.62	16.12	Uncl*	1.26	Uncl	dK7	K0III	140	1.23	0.305	32
239630	296.332458	–14.951111	17.76	16.91	16.48	C*	1.49	C:	C5.5	C	800	1.237	0.408	11
239687	296.034485	–14.951339	17.57	16.71	16.39	M*	2.10	C	C3.2	K0IV	22	1.162	0.44	11
242030[4]	296.345795	–14.960103	16.91	16.07	15.72	M	1.61	C:	C5.5	C	819	1.181	0.423	21
248633	296.33786	–14.988564	16.73	15.73	15.19	C*	1.79	C:	C3.2	S	809	1.443	0.402	11
248651[4]	296.281311	–14.988667	17.16	16.35	16.07	M	1.63	C	C5.5	C	682	1.147	0.426	14
165760	296.204498	–14.674287	18.32	17.55	17.28	M	1.14	C	dK7	K0III	292	1.117	0.553	10
177839	296.247101	–14.722958	18.13	17.27	17.03	M	0.69	C	dK7	K4III	526	1.192	0.446	12
187649[1,4]	296.244446	–14.75467	17.25	16.49	16.22	M	0.42	C:	dK7	K0IV	503	1.141	0.313	18
188333	296.350891	–14.757086	16.98	16.22	15.85	M*	1.02	C:	dK7	K0III	826	1.171	0.414	29
191318[1]	296.234558	–14.767653	16.96	16.04	15.62	C*	0.30	C	dK7	K3III	461	1.342	0.574	19
193220	296.290405	–14.774523	17.63	16.84	16.69	M	0.50	Ce:	dK7	K0III	718	1.139	0.385	11
194777[3]	296.278412	–14.780069	17.65	16.54	15.76	C*	0.39	Ce:	dK7	K0IV	668	1.691	0.565	14
194949	296.352264	–14.780713	17.09	16.30	15.76	C*	0.97	C:	dK7	K0III	828	1.325	0.518	22
195133[1]	296.229034	–14.781347	17.61	16.51	15.94	C*	0.20	Ce:	dK7	K0III	435	1.39	0.532	22
195884[1]	296.213776	–14.783867	17.89	17.08	16.72	M	0.26	C	dK7	K0IV	333	1.247	0.443	22
198595[1]	296.257843	–14.793209	17.91	17.14	16.88	M	0.19	Ce:	dK7	K0III	575	1.218	0.334	19
199754[1]	296.208191	–14.797331	17.67	16.91	16.45	C*	0.25	Ce	dK7	K0III	309	1.138	0.338	16
200300	296.184326	–14.799191	17.83	17.03	16.78	M	0.44	Ce:	dK7	K4III	224	1.104	0.369	15
200573	296.274109	–14.800164	17.57	16.75	16.40	M	0.30	Ce	dK	K0III	653	1.2	0.41	13
201454[1]	296.251343	–14.803117	17.41	16.50	16.15	C*	0.11	Ce:	dK7	K0III	544	1.41	0.512	27
204144	296.404907	–14.812469	0.00	16.54	16.16	Uncl*	1.39	C	dK7	K4III	863	1.16	0.406	16
205865	296.191315	–14.818703	16.95	16.05	15.64	C*	0.41	Ce	dK7	K4III	244	1.275	0.528	15
207586[1]	296.212616	–14.82485	17.39	16.56	16.25	M	0.28	C	dK7	K0IV	327	1.119	0.419	17
208714	296.182983	–14.828946	17.60	16.81	16.58	M	0.50	Ce	dK7	K0III	219	1.118	0.383	18
209216[1]	296.233093	–14.830748	17.39	16.60	16.31	M	0.24	Ce	dK7	K0III	458	1.118	0.397	18
213379[3]	296.241516	–14.846167	18.41	17.30	16.36	C*	0.37	Ce:	dK7	K0III	489	1.215	0.365	11
217716	296.234772	–14.862573	17.71	16.99	16.68	M	0.51	Ce:	dK	K0V	466	1.221	0.404	12
223739	296.153625	–14.886689	18.00	17.21	16.92	M	1.00	C	dK7	K0III	131	1.161	0.393	10
242563	296.183685	–14.962144	18.24	17.33	16.82	C*	1.43	C	dK	K0IV	222	1.21	0.478	12

Table 11. 73 candidate AGB sources in the outer region (≥5 kpc) for which spectra have been obtained.

ID	RA (2000.0) (deg)	Dec (2000.0) (deg)	J (mag)	H (mag)	K (mag)	Phot. type	Dist. (kpc)	Spec. type	Kmatch	Dmatch	S/N
12243	296.358276	–13.897025	17.58	16.84	16.62	M	7.81	dM:	dM3.5	M1.5V	13
20479	296.329987	–13.938492	17.49	16.72	16.70	M	7.43	dK	dK7	K0III	20
27278	296.079315	–13.973788	17.74	16.98	16.90	M	7.21	dM:	dM3	M3V	16
29959	296.396942	–13.987878	17.15	16.41	16.30	M	7.10	dM:	dM0	M0V	13
35137	296.6521	–14.015325	18.33	17.57	17.32	M	7.56	dK:	dK7	K4III	11
38421	296.7117	–14.03266	18.29	17.56	17.35	M	7.67	dK:	dK7	K2V	14
63349	296.484314	–14.154216	18.15	17.16	16.43	C	5.91	dK	dK	K0V	11
64581	295.60434	–14.160067	17.65	16.92	16.73	M	7.60	dM:	dM1.5	M0V	13
67487	296.492676	–14.174297	17.46	16.71	16.57	M	5.78	dM:	dM2	M1.5V	11
78272	296.068665	–14.228847	17.94	17.21	17.00	M	5.11	dM:	K7III	M0V	11
78560	295.52533	–14.230219	17.56	16.80	16.77	M	7.67	dK	dK7	K2V	19
81011	296.979736	–14.242464	17.83	17.11	16.91	M	7.80	dM	dM3.5	M3V	10
83584	296.461334	–14.256592	17.03	16.29	16.12	M	5.03	dM:	dM1.5	M1.5V	16
86214	295.588501	–14.270535	17.46	16.72	16.56	M	7.04	dM	dM0	M0V	17
88989	295.462524	–14.283733	17.55	16.81	16.63	M	7.80	dM	dM1.5	M0V	12
89016	295.571045	–14.283828	17.75	16.98	16.86	M	7.08	dM:	dM1.5	M3V	11
107892	295.808746	–14.380803	17.90	17.17	17.08	M	5.06	dK	dK7	K0III	13
112177	296.821106	–14.404108	17.67	16.93	16.79	M	5.91	dM:	dM1.5	M1.5V	13
117401	297.100342	–14.432428	18.51	17.75	17.34	M	7.81	dK:	dK	K0V	14
127636	296.787109	–14.488456	17.80	16.99	16.77	M	5.28	dK:	dK7	K2V	11
128222	297.023987	–14.491783	17.85	17.05	17.02	M	7.03	dM:	dM3.5	M3V	11
140011	296.800354	–14.549609	17.48	16.73	16.57	M	5.14	dM:	dM3.5	M3V	12
143954	295.40918	–14.567859	18.05	17.24	17.14	M	7.14	dM	dM0	M0V	11
146932	297.072693	–14.582489	17.77	17.04	16.86	M	7.16	dM:	dM0	M0V	13
148616	296.853027	–14.590661	18.26	17.49	17.34	M	5.41	dK:	dK7	K0III	13
152918	296.812988	–14.611956	18.19	17.45	17.19	M	5.03	C:	C3.2	C	11
155389	297.11145	–14.624125	17.25	16.50	16.37	M	7.39	dM:	dM1.5	M0V	21
157802	296.911255	–14.636194	17.79	17.06	16.91	M	5.75	dK:	dK7	K0III	16
165107	297.148376	–14.671167	17.74	17.01	16.82	M	7.62	dM:	dM1.5	M1.5V	11
184165	295.609711	–14.742889	17.68	16.96	16.69	M	5.22	dM:	dM3.5	M3V	12
185402	295.516144	–14.746992	16.85	16.11	15.87	M	5.99	dMe	dM1.5	M3V	32
200928	295.559082	–14.801364	17.60	16.82	16.65	M	5.61	dMe:	dM0	M0V	19
201578	295.527863	–14.803578	17.05	16.29	16.12	M	5.87	dMe:	dM1.5	M3V	25
201803	295.621918	–14.804337	17.94	17.17	16.95	M	5.09	dM:	dM1.5	M3V	11
208174	295.512543	–14.826831	17.85	17.13	17.01	M	6.00	dMe	dM1.5	M0V	16
215764	295.524353	–14.855192	18.01	17.16	17.11	M	5.91	dMe:	dM1.5	M0V	10
220386	295.535919	–14.873045	17.77	17.04	16.99	M	5.83	dK	dK7	K0IV	19
223551	295.621216	–14.885853	18.13	17.32	17.13	M	5.14	dK	dK7	K0III	13
223794	295.547546	–14.886919	17.05	16.32	16.13	M	5.75	dM	dM3.5	M3V	20
234263	295.540558	–14.933914	17.48	16.74	16.64	M	5.87	dM:	dM1.5	M0V	17

Notes. In Col. 9 the use of "d", "e" and ":" have the same meaning as in Table 10. A further four sources which showed high energy emission lines are listed in Table 4.

Table 11. continued.

ID	RA (2000.0) (deg)	Dec (2000.0) (deg)	J (mag)	H (mag)	K (mag)	Phot. type	Dist. (kpc)	Spec. type	Kmatch	Dmatch	S/N
246831	295.639313	–14.980222	17.65	16.92	16.77	M	5.17	dK:	dK7	M0V	11
254251	295.404724	–15.01522	16.36	15.60	15.48	M	7.12	dK	dK7	K2V	31
276398	295.72052	–15.125569	17.63	16.68	16.07	C	5.08	C:	C6.5	C	13
277183	295.640228	–15.129666	16.22	15.48	15.26	M	5.67	dM	dM1.5	M3V	23
286135	295.417267	–15.171911	17.02	16.30	16.09	M	7.48	dM	dM0	M0V	12
289833	295.405945	–15.189603	16.94	16.17	16.03	M	7.62	dK	dK7	K0IV	30
292760	296.767883	–15.204441	15.14	14.40	14.22	M	5.57	dM	dM2	M1.5V	70
297583	295.799805	–15.229388	17.06	16.31	16.16	M	5.14	dM	dM0	M0V	39
298121	295.47818	–15.232033	17.00	16.27	16.15	M	7.27	dM:	dM1.5	M3V	14
299996	295.776978	–15.241439	18.24	17.41	17.25	M	5.34	C:	C3.2	S	10
303122	295.743439	–15.257809	18.33	17.57	17.29	M	5.64	dM	dM0	M0V	12
305736	295.49173	–15.271272	17.58	16.83	16.68	M	7.35	dK	dK7	K0IV	13
309370	295.872925	–15.289667	17.27	16.44	16.29	M	5.14	dM	dM1.5	M3V	18
312062	295.534882	–15.303519	17.08	16.33	16.18	M	7.21	dM:	dM1.5	M3V	17
312215	295.499207	–15.304358	17.58	16.76	16.75	M	7.45	dK	dK7	K0IV	14
313097	295.87912	–15.309017	17.90	17.11	16.88	M	5.24	dK	dK7	K2V	15
317557	295.794037	–15.329094	17.83	17.03	16.78	M	5.80	dK:	dK7	K0IV	14
317678	295.949036	–15.329528	18.11	17.33	17.07	M	5.09	dM:	dM0	M0V	11
318572	295.576233	–15.333383	16.93	16.21	16.05	M	7.10	dK	dK7	M0V	23
319631	295.897827	–15.337833	17.39	16.57	16.39	M	5.37	dM:	dM3.5	M3V	26
324005	295.537048	–15.357962	17.10	16.37	16.11	M	7.48	dM:	dM4.5	M3V	11
324064	295.966644	–15.358248	18.35	17.40	17.07	C	5.25	dM:	dM2	M1.5V	11
327377	296.011719	–15.374639	17.91	17.10	17.16	M	5.23	dK	dK7	K2V	14
329347	295.516876	–15.380892	17.16	16.36	16.24	M	7.74	dM:	dM1.5	M0V	15
330842	296.342438	–15.386158	18.09	17.26	17.22	M	5.06	dM	dM1.5	M3V	12
332677	295.648956	–15.39533	17.62	16.89	16.70	M	7.02	dM:	dM1.5	M0V	14
344297	296.123199	–15.455264	17.35	16.60	16.47	M	5.66	dM	dM1.5	M1.5V	12
344467	296.182312	–15.456194	17.68	16.95	16.80	M	5.60	dK	dK7	K0V	23
346806	296.019073	–15.468775	18.21	17.31	16.65	C	5.97	Uncl	dK7	K0IV	11
350411	295.58786	–15.487622	17.33	16.58	16.51	M	7.94	dK	dK7	K3III	15
355390	295.772949	–15.513988	17.73	17.01	16.74	M	7.19	dM:	dM3	M1.5III	14
366911	296.781189	–15.567519	17.99	17.20	17.12	M	7.93	dM	dM0	M0V	10
368750	296.538513	–15.576294	17.82	17.06	16.87	M	7.06	dM:	dM1.5	M1.5V	12

Table 12. 43 candidate AGB sources in the inner (top) and outer (bottom) regions for which we are able to offer a tentative classification despite the low S/N of the spectra obtained.

ID	RA (2000.0) (deg)	Dec (2000.0) (deg)	J (mag)	H (mag)	K (mag)	Phot. type	Dist. (kpc)	Spec. type	Kmatch	Dmatch	Letarte ID	$R-I$ (mag)	CN–TiO (mag)	S/N
158986	296.190338	–14.641755	17.59	16.78	16.40	M	1.43	C	C5.5	C	239	1.196	0.366	8
164010	296.32608	–14.666169	17.58	16.80	16.51	M	1.38	C	C5.5	C	792	1.116	0.339	9
167230[4]	296.335388	–14.681108	18.39	17.51	17.10	C*	1.32	C	C5.5	C	804	1.276	0.402	10
170004	296.110596	–14.693192	0.0	16.87	0.0	Uncl*	1.41	C	dK7	K0IV	80	1.426	0.67	9
172060	296.196411	–14.702325	17.75	16.37	15.10	C*	0.93	dK	dK7	K0IV	258	1.848	0.507	9
172656	296.539612	–14.704988	17.59	16.48	15.73	C*	2.64	C	C5.5	C	900	1.594	0.531	7
173378	296.099152	–14.708244	17.48	16.63	16.27	C*	1.40	C	C5.5	C	64	1.171	0.454	10
174035	296.374054	–14.711063	17.55	16.85	16.52	M*	1.38	C	C	C	845	1.12	0.414	7
174226	296.075775	–14.711885	18.14	17.39	17.10	M	1.55	C	C	C	42	1.158	0.373	8
174472	296.341431	–14.712852	17.32	16.39	15.85	C*	1.16	C	C5.5	C	814	1.355	0.558	10
178893	296.110779	–14.725801	17.15	16.18	15.45	C*	1.24	C	C6.5	C	82	1.48	0.456	9
179183	295.977081	–14.726664	17.58	16.77	16.22	C*	2.25	C	C5.5	C	7	1.255	0.423	8
183391	296.08786	–14.740214	17.23	18.14	15.90	C*	1.35	C	C6.5	C	53	1.266	0.37	10
184858[4]	296.171387	–14.745203	18.02	17.23	16.97	M	0.74	C	dK7	K4III	181	1.121	0.375	8
186954	296.469086	–14.752255	0.0	17.74	16.28	Uncl*	1.96	dK	dK	K2V	887	1.931	0.415	10
190283	296.342804	–14.764064	18.20	17.41	17.02	M	0.93	C	C5.5	C	815	1.222	0.354	7
191195	296.106384	–14.767224	17.62	16.80	16.58	M	1.13	C	C5.5	S	72	1.183	0.425	8
191382	296.304626	–14.767883	17.76	17.03	16.59	M*	0.63	C	C	K0III	759	1.124	0.455	8
192177	296.333038	–14.770712	18.24	17.51	17.25	M	0.84	C	C3.2	C	803	1.194	0.392	8
207096	296.162018	–14.82305	17.45	16.64	16.28	M	0.65	C	C5.5	C	154	1.176	0.544	9
212351	296.167816	–14.842195	17.72	16.99	16.60	M	0.67	C	C	K0III	169	1.122	0.438	10
212970	296.066071	–14.844581	17.44	16.78	16.30	M*	1.46	C	C5.5	C	34	1.151	0.446	10
218420	296.364624	–14.865284	17.45	16.57	16.19	C*	1.18	C	C3.2	C	836	1.155	0.478	9
219598	296.297241	–14.869897	17.49	16.70	16.21	C*	0.76	C	C5.5	C	747	1.129	0.375	10
226097[4]	296.207458	–14.896397	17.39	16.58	16.20	M	0.84	C	C5.5	C	308	1.179	0.564	10
229856	296.368011	–14.913227	16.96	15.87	15.15	C*	1.43	C	C5.5	S	839	1.701	0.356	7
237395	296.070709	–14.94352	0.0	18.45	0.0	Uncl*	1.83	C	dK	K0III	37	1.349	0.441	6
237999	296.08905	–14.945495	18.64	0.0	15.90	C*	1.73	C	C5.5	C	54	1.588	0.303	7
240673	296.06134	–14.955141	18.23	17.20	17.10	M*	1.95	C	C5.5	C	31	1.263	0.442	8
245610[2]	295.969788	–14.97507	17.69	16.93	16.60	M	2.66	C	C5.5	C	5	1.161	0.42	8
250173	296.215485	–14.99597	0.0	18.06	16.76	Uncl*	1.66	C	C5.5	K0V	342	1.305	0.445	7
253239	296.090485	–15.010141	18.20	16.77	16.74	C*	2.15	C	C5.5	C	56	1.199	0.37	9

Notes. The columns are the same as those in Table 10. In Col. 1 those sources with a superscript are in common with the catalogues of [(2)] Demers et al. (2006) and [(4)] Kacharov et al. (2012, see Table 13). In Col. 9 the use of "d" has the same meaning as in Table 10. In Col. 12 for the outer region sources there is no ID number given for the catalogue of Letarte et al. (2002).

Table 12. continued.

ID	RA (2000.0) (deg)	Dec (2000.0) (deg)	J (mag)	H (mag)	K (mag)	Phot. type	Dist. (kpc)	Spec. type	Kmatch	Dmatch	Letarte ID	$R-I$ (mag)	CN–TiO (mag)	S/N
21034	296.250183	–13.941045	18.11	17.39	17.26	M	7.37	dK	dK7	K0V	–	0.0	0.0	8
32087	296.552612	–13.999165	17.52	16.76	16.61	M	7.36	dK	dM0	M0V	–	0.0	0.0	8
62395	296.365326	–14.149378	17.16	16.39	16.28	M	5.69	dM	dM1.5	M1.5V	–	0.0	0.0	9
98241	296.653442	–14.330378	17.62	16.87	16.78	M	5.31	dM	dM2	M1.5V	–	0.0	0.0	9
101637	295.688538	–14.347858	18.14	17.41	17.14	M	5.98	dM	K7III	M0III	–	0.0	0.0	8
222762	295.594513	–14.882525	17.85	17.06	16.80	M	5.36	dM	dM3.5	M3V	–	0.0	0.0	10
302586	297.015076	–15.255167	18.22	17.49	17.35	M	7.50	dM	dM2	M1.5V	–	0.0	0.0	7
303607	295.81015	–15.260356	18.27	17.55	17.34	M	5.27	dM	K7III	K4III	–	0.0	0.0	7
334393	296.061401	–15.403897	17.71	16.95	16.74	M	5.34	dM	dM3.5	M3V	–	0.0	0.0	8
337831	295.923065	–15.421967	18.42	17.67	17.39	M	5.90	dK	dK7	K0IV	–	0.0	0.0	10
372253	295.796112	–15.593744	18.17	17.44	17.29	M	7.68	dK	dK7	K0IV	–	0.0	0.0	8

Table 13. Spectral source counterpart IDs.

ID	Kang et al. (2006)	Demers et al. (2006)	Kacharov et al. (2012)	Whitelock et al. (2013)
167 230	–	–	77 470	–
168 826	–	–	78 095	–
184 858	–	–	83 752	–
187 649	338	–	84 882	–
188 246	–	–	85 162	–
188 974	–	1087	–	–
191 318	591	–	–	–
194 777	–	–	–	11 271
195 133	581	–	–	–
195 884	79	–	–	–
198 595	474	–	–	–
199 754	39	–	–	–
201 454	409	–	–	–
206 129	298	–	–	–
207 586	70	–	–	–
209 216	248	–	–	–
209 650	–	1084	–	–
209 652	–	1056	–	–
213 379	–	–	–	11 764
225 648	–	–	102 136	–
226 097	–	–	102 365	–
226 603	–	–	102 622	–
228 306	–	–	103 500	–
242 030	–	–	108 813	–
245 610	–	1020	–	–
248 651	–	–	111 423	–

Notes. For those sources in Tables 10 and 12 which we have matched with a source elsewhere in the literature, we now provide the identification number for the corresponding source in the catalogues of Kang et al. (2006), Demers et al. (2006), Kacharov et al. (2012); and Whitelock et al. (2013).